Presented at the Relativistic
Heavy-Ion Physics Symposium,
GSI, Darmstadt, West Germany,
March 5-8, 1978

LBL-7730 c.2

SINGLE PARTICLE INCLUSIVE AND CORRELATION MEASUREMENTS

H. H. Gutbrod

May 1978

Prepared for the U. S. Department of Energy
under Contract W-7405-ENG-48

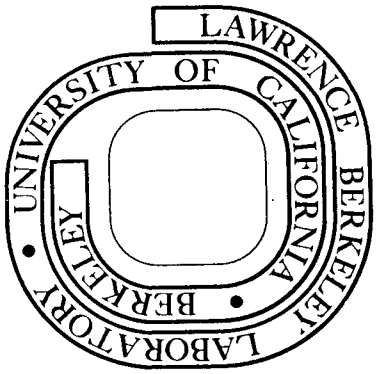

DISCLAIMER

SINGLE PARTICLE INCLUSIVE AND CORRELATION MEASUREMENTS

H. H. Gutbrod

GSI, Darmstadt
West Germany

and

Lawrence Berkeley Laboratory
University of California
Berkeley, California 94720

I. INTRODUCTION

Despite the complex nature of a central collision of a relativistic heavy ion with a target nucleus as previously discussed by Prof. Schopper and shown in Fig. 1, there are reasons why detailed single particle studies have to be done. By measuring precisely the double differential cross sections one collects information on the average multiplicity of such a reaction and one obtains the details of energy and momentum dissipation on the average in the reaction observed. Furthermore, if the particles detected are clusters there is information on the correlation of nucleons and the formation process. A comparison of single particle inclusive data with theories will be the first part of the talk.

Our major interest, however, is to study central collisions where density effects are expected, where density isomers may be produced -- in short where interesting new physics is expected. For that investigation, single particle inclusive spectra are not conclusive enough since we do not know what kind of particle originates only from central collision (e.g., in low energy heavy ion physics the evaporation residues are a clear small impact parameter trigger). If density isomers do not exist with a long life-time -- or not at all -- then

there is agreement that high multiplicity events are related to small impact parameters -- the higher the multiplicity of charged particles, the smaller the impact parameter.

Therefore we obtained single particle inclusive data together with associated charged particle multiplicities in order to see the features of the total event, e.g. like forward peaking, asymmetries, and shapes of the multiplicity distribution. This will be the second part of this report.

II. THEORETICAL APPROACHES

This report excludes a discussion of the various models which have been developed during the last two years and which are discussed in the following talks. But a short characterization seems to be appropriate. There are first simple models like the Fireball, the Firestreak, and Row-on-Row. They describe the geometrical and kinematical aspects of the entrance channel and assume the validity of thermodynamics during and after the collision of projectile and target.

In Fig. 2 the nuclear fireball[1] at one impact parameter is pictured emitting particles isotropically in its rest frame. If one assumes a Maxwell Boltzmann distribution (Fig. 3a) for the emission from a hot volume with temperature τ, the velocity of the system leads to a spread of the spectra with angle (Fig. 3b) which increases with increase in velocity (Fig. 3c). This model has been refined by W. D. Myers to the Firestreak model[2] which conserves also angular momentum (Fig. 4). The Firestreak model was further pushed by J. Gosset, J. Kapusta, and G. Westfall[3] to include formation and emission of clusters in the chemical equilibrium formalism developed by A. Mekjian,[4] which I will discuss later.

Whereas simple models like fireball-firestreak, etc., exclude dynamical effects like compression or collective excitations, those are explicitly included in macroscopic models like the relativistic fluid dynamics model and the relativistic two-fluid dynamics model to be presented by R. Nix[5] in a following talk. Disregarding the question of validity of hydrodynamics in nuclear reactions, there are predictions of observable effects, like shock-waves, etc., as shown in Fig. 5. Calculations by R. Nix et al[5] show for impact parameters of 0.5 a strong deflection of the projectile and the matter pushed out of the target nucleus. Furthermore a kind of shock propagates into the spectator equal to the target rest giving it a kick into the transverse direction.

A microscopic description is approached in two different ways, a) via a relativistic intranuclear cascade calculation,[6] and b) by solving the nonrelativistic many-body equations of motion.[7] These subjects will be presented in the afternoon session.

As pointed out already several times in the preceding talks, a model-independent presentation of the data is desired to obtain hints of the mechanism involved. A contour plot of the invariant cross section $1/p\ d^2\sigma/dEd\Omega$ in a plane of $p_\perp/m$ versus rapidity $y = 1/2\ \ln[(E+p_\parallel)/(E-p_\parallel)]$ allows one to differentiate reaction products via rapidity space. Products around y=0 are predominantly target fragments, whereas products y_{Beam} are called projectile fragments. A special feature of such a presentation is that when fragments are emitted isotropically from a unique moving source then the contours will center around the rapidity of this source. We will use this feature in the upcoming discussion.

In the following single-particle inclusive data will be presented, afterwards we include associated multiplicities and two-particle inclusive correlations of fragments.

III. SINGLE PARTICLE INCLUSIVE DATA

Pions

The observation of pions promises some information on their production mechanisms, i.e. whether they are produced in primary nucleon-nucleon collisions, or whether they are generated in the decay of resonances. If all oberved pions came from the decay of resonances then the pion spectrum would drop to zero kinetic energy.[8] In Fig. 6 data of K. Nakai et al[9] for π^+ , and in Fig. 7 of S. Nagamiya et al[10] for π^- are presented and compared to calculations based on a superposition of nucleon-nucleus data. Deviations of a factor of two or more question the values of such a phenomenological approach. In Fig. 8 and 9 a comparison of π^- production (presented as contours of invariant cross sections in a $p_\perp$/m-y plane) for ^{12}C on ^{12}C and ^{12}C on Pb show for large pion energies a minimal deviation from nucleon-nucleon kinematics when going from a carbon target to a Pb target. There is, however, a deviation visible at low pion moments. Figure 10 shows pion yields at various angles as a function of target mass. No simple explanation for the strong A dependence can be given today. All experiments of single-pion inclusive measurements indicate that there is at low energies (100-250 MeV/u) no copious pion production.

Protons

While the pions do not show kinematical effects as a function of masss asymmetry in the entrance channel, the proton spectra show a large difference between the C on C and the C on Pb system (Fig. 11, data of Nagamiya et al[10]). At low $p_\perp$ values the rapidity of the apparent source shifts to much lower values than that of the nucleon-nucleon system indicated by $(y_p + y_1)/2$. The strong influence of kinematics is further visible in Fig. 12, where the integrated yield of protons at various lab-angles is compared as a function of target mass.

Whereas at forward angles the proton yield follows the geometrical cross section, the behavior at back angle has a much stronger A-dependency.

Our own data of proton-inclusive measurements are shown in Fig. 13.[11] The double differential cross sectrion show smooth curves which fall off exponentially at large angles. As pointed out in the introduction we may start an analysis of the data by comparing them to a "temperature + velocity" model such as the fireball or firestreak model. In Fig. 14 we see that in comparison the firestreak calculation[3] produces a larger yield at forward angles than the experiment, whereas beyond 60° the experimental yields are larger than the calculated ones (i.e. there is less forward peaking and more sideways flux observed than described in the firestreak model). Note, that these are still single-particle inclusive data, where all impact parameter contribute, predominantly the large ones.

Light Fragments (d,t → Oxygen)

In Fig. 15 the double differential cross sections for p,d,t ^{3}He and ^{4}He are shown; in Fig. 16 those for Li up to oxygen.[1] As the fragment mass increases, the slope of the double differential cross section gets steeper and for fragments above ^{4}He, all spectra fall off exponentially. For all fragments the double differential cross section decreases with increasing angle.

In high-energy reactions the probability of finding a deuteron was calculated as the probability of finding a proton (given by the single particle cross section of protons) times the probability of finding a neutron within a sphere of radius p_o around the momentum p of the proton.[12] This idea was taken up and applied to cluster formation in heavy-ion reactions.[13] The single-particle inclusive cross section of a particle with n nucleons

is then written as

$$\frac{d^2\sigma_n(p)}{p^2 dp d\Omega} = \frac{1}{n!}\left(\frac{4\pi}{3}\frac{p_o}{\sigma_o}\right)^{n-1}\left(\frac{d^2\sigma_1(p)}{p^2 dp d\Omega}\right)^n$$

where σ_o is the reaction cross section. In Fig. 17 data are compared with these final state calculations for d,t, ^{3}He, ^{4}He, and in Fig. 18 for Li and Be. The values for p_o are around p_o = 135 MeV/c.

Since the spectra fall off exponentially, we can picture the clusters originating from a temperature bath with temperature τ, where they are in a chemical equilibrium. This model as outlined, also by Mekjian[4], yields quite reasonable fits to the data as shown in Figs. 19 and 20.

Summarizing the single-particle inclusive data -- the first part of this talk -- we can state the following observations:

1) The pions are produced most probably in primary n-n collisions. At low pion energies (E_π < 100 MeV) the contributions from the decay of resonances are not easy to detect. There is more data needed on pion production, specifically in the low pion energy region where, in principle, kinematical effects different from n-n collisions could be detected.

2) There exist a power-law relationship between cluster cross section and proton cross section, which can be explained by final-state interaction or chemical equilibrium giving information on a freeze-out density.

3) Therefore, the proton spectra have to be understood as a key element to the primary reaction mechanism

a) For 40 $\leq E_p \leq$ 200 MeV, the proton yield is roughly constant at forward angles (20°-30°) when going from 400 MeV/nucleon to 2100 MeV/nucleon, ^{20}Ne or U, but increases by a factor of 10 at 130°.

b) The proton yield as a function of the target mass increases much more at back angles than at forward angles.

c) Much more transverse flux is experimentally observed than predicted in the fireball or firestreak model.

Let us turn now to more complex measurements where we hope to learn more about the mechanism of relativistic heavy-ion reactions.

IV. CORRELATION MEASUREMENTS

In the previous section we touched already one kind of correlation leading to the formation of clusters and light nuclei. I will not go any further into that small-angle nucleon-nucleon correlation, but rather, taking a large viewpoint of the word correlation, discuss in the following the charged particle multiplicity associated with various single-particle data, its θ and ϕ distribution, and by that look into decay patterns and correlations.

In Fig. 21 the experimental apparatus we used is shown as it is set up. The solid state counter telescope consists of two ΔE silicon detectors and and intrinsic germanium E counter of 7 cm length, long enough to stop 200 MeV protons. Associated with these telescope events, we measure outside of the scattering chamber in 80 scintillators, reaction products with an energy above that of 25 MeV protons. The scintillators are grouped in four rings at different angle θ, ring A from 9°-20°, ring B from 20°-45°, ring C from 45°=80°, and ring D from 120°-160°. This allows one to get a rough idea of the distribution in θ, whereas we get more detailed information from ϕ. Compared with an emulsion analysis we are looking with our multiplicity array at the θ and ϕ distribution of the grey shower particle. Figure 22 shows the sensitivity of the various detector rings A,B,C,D projected into the $(y\text{-}p_{\perp}/m)$ plane. Ring A might see contributions from the projectile rapidity, ring B

covers the mid-rapidity region, and ring C and D see mostly fragments at target rapidity.

Let us now have a look at the measured associated multiplicities as a function of the target. In Fig. 23, for ^{20}Ne projectiles, the average multiplicity for ring A associated with a proton ($30 \leq E_p \leq 200$ MeV) at 400 MeV/nucleon does not change and at 2.1 GeV/n, changes little as we go up from ^{20}Ne on ^{27}Al to ^{20}Ne on U. We interpret this as being a spray of projectile-nucleons in violent peripheral reactions which appear to be nearly target-independent. A strong increase in multiplicity as function of target mass can be seen in ring B and C, which are sensitive to the mid-rapidity region adn the target-rapidity region.

In Fig. 24a the average multiplicities are shown for various projectiles on a U target at 400 MeV/n and 1050 MeV/n. One observes a constant increase of charged particle multiplicity with the increase of Z of the projectile. Note that the strongest increase is found in ring B which subtends the angular region of 20° to 45°. Figure 24b shows the strong linear increase of the average total multiplicity of charged particles as a function of projectile mass.

Since we started out with the assumption of "the higher the charged particle multiplicity, the smaller the impact parameter" we are interested in observing a difference between events with high and low associated multiplicity. In Fig. 25a the double differential cross section for protons from ^{20}Ne or U at 400 MeV/n is shown for high multiplicity, i.e. more than 12 scintillation counters had to have fired, and in Fig. 25b data are shown for low multiplicity events, i.e. events where less than 6 scintillators fired. We see a large difference -- the low multiplicity events are much more forward peaked than the high multiplicity events, whose spectra are more clustered

together for the various angles. In both cases we selected about 10% of the observed cross section. In Fig. 26 we illustrate the observed fact again by looking at the multiplicity angular distribution of the average events in our selection. The low multiplicity event is typically strongly forward peaked, i.e. the pattern is that of a narrow shower limited to small angles, whereas the high multiplicity event has 10 times more fast charged particles emitted into the backward hemisphere. Thus a high multiplicity event is characterized by a large dissipation of the projectile energy into transverse direction, whereas the low multiplicity event (the peripheral reaction) still contains a predominantly longitudinal component due to the projectile fragments.

Let me come now to an experiment[14] we just finished recently, where indeed, we found a trigger particle produced only in very violent collisions. In the reaction of 400 MeV/n ^{20}Ne on U, Au and Ag, slow target fragments were measured from Be up to fission-like events. Using a ΔE ionization chamber and silicon E detectors, five solid-state coincident counters were placed opposite to the telescope and measured in-plane- and out-of-plane-correlated slow fragments. The experimental setup is shown in Fig. 27. The multiplicity measurement was accomplished as previously described.

Figure 28 shows the multiplicity distributions in ring B for various trigger particles: fission-like events from ^{20}Ne on U at 400 MeV/n indicate a clear peripheral reaction with strong enhanced contribution of low multiplicities; a slow alpha particle (20-60 MeV) has about the same associated multiplicity distribution as do pions, protons, deuterons, and tritons measured in the solid-state telescope described above. The slow oxygen particles, however, show an absence of low multiplicities at this bombarding energy and for such a target-projectile combination. Looking onto the average total multiplicity as a function of the mass of the trigger particle (Fig. 29)

we observe a maximum for Z in the range of 8 to 12. For the first time this is direct proof of earlier findings by Poskanzer[15] in proton bombardment, that medium-heavy target fragments are originating from very violent reactions (Ref. 15 describes reactions with very high temperature components). Our observation stresses this point further by pointing out that peripheral collisions associated with low charged-particle production contribute little or not at all to the formation of these fragments. The reaction mechanism for the production of these slow nuclear fragments is not clear, specifically, if we look at the reaction ^{20}Ne on Ag at 400 MeV/n. The multiplicity is so high that there is not enough charge left to account for a very asymmetric fission-like process. Furthermore, we do not observe a coincident particle correlated at an angle between 120° to 180° (which we do for the fission events) with an energy above 6 MeV (11 MeV would be the smallest energy of a Z=29 fragment correlated at 180° to an observed Ne particle in the telescope; lighter correlated fragments would have higher energy to balance the momentum of a 40 MeV ^{20}Ne).

In Fig. 30 we look at the ϕ correlation of the shower particles with the trigger particle. We observe for the heavy masses with $Z \geqslant 13$ a clear 180° correlation, i.e. an in-plane correlation between one heavy reaction product and the whole shower of fast charged particles. It is interesting to compare this observation qualitatively with the hydrodynamical predictions shown in Fig. 5 and consider collective effects to be responsible for the sidekick of the shattered projectile and of the target remnant.

V. SUMMARY

After several years of experimental investigations there is quite a substantial increase in overall knowledge. Many facts are observed and some fictions have vanished. The theoretical understanding of what is going on in relativistic nuclear collisions is growing, but as so often in science, models are good as long as there are no contradicting data for comparison.

More new single-particle data with higher precision than the early ones help to weed out the various models of relativistic nuclear collisions. We have observed experimentally more flux into the transverse direction than predicted by the fireball (firestreak model) which we consider to be a very helpful first-order description of the trivial or averaged phenomena, a kind of standard which allows us to see more easily phenomena other than of simple thermalization (which in itself is a highly interesting subject, since equilibrium times would be extremely short and temperatures reaching the limiting temperature[16]).

There are no new theoretical attacks on the cluster production data, only the old ones,[4,13] where there is still a difference in the underlying physics. Are the clusters formed only at the freeze-out density via final state interaction or are they in chemical equilibrium in the hot reaction volume?

For the first time a selection on the associated charged particle multiplicity yields distinctive trends in the double differential cross sections. High multiplicity events have double differential cross sections which are less spread apart with angle than the much more forward peaked low multiplicity events. An analysis of these central events is in full process and we hope to come closer to the often demanded study of very small impact parameter reactions.

The observation of ϕ correlations -- a 180° enhancement of coincident fast particles -- guides the interest to violent peripheral reactions. Perhaps it will be in these reactions that we detect (or have detected?) compression effects.

ACKNOWLEDGMENTS

I would like to thank all my colleagues for their support and enthusiasm, specifically W. G. Meyer, A. M. Poskanzer, A. Sandoval and R. Stock, who helped with many discussions and comments. I am much indebted to R. Bock for his continuous interest and support.

This work was done under the auspices of the U.S.Department of Energy and the Bundesministerium für Forschung und Technolgie, West Germany.

REFERENCES

1. J.Gosset, H.H.Gutbrod, W.G.Meyer, A.M.Poskanzer, A.Sandoval, R.Stock, G.D.Westfall, Phys. Rev. C16, 629 (1977).
2. W.D.Myers, Nucl. Phys. A296, 177 (1978).
3. J.Kapusta, G.Westfall, and J.Gosset (to be published, 1978).
4. A.J.Mekjian, Phys. Rev. Letters 38, 604 (1977).
5. A.A.Amsden, G.F.Bertsch, F.H.Harlow, J.R.Nix, Phys. Rev. Lett. 35, 905 (1975); A.A.Amsden, F.H.Harlow, J.R.Nix, Phys Rev. C15, 2059 (1977); A.A.Amsden, A.S.Goldhaber, F.H.Harlow, J.R.Nix, LASL preprint LA-UR-77-2961.
6. R.K.Smith, M.Danos, Proceedings of Meeting on Heavy-Ion Collisions, Fall Creek Falls, Tennessee (June 1977), and to be published.

7. A.R.Bodmer, C.N.Panos, Phys. Rev. C15, 1342 (1977); A.R.Bodmer, Proceedings of the Meeting on Heavy-Ion Collisions, Fall Creek Falls Tennessee (June 1977); and L.Wilets, E.M.Henley, M.Kraft, and A.D.MacKellar, Nucl. Phys. A282, 341 (1977).

8. J.Kapusta, Lawrence Berkeley Laboratory preprint LBL-6504 (1977).

9. K.Nakai, J.Chiba, I.Tanihata, S.Nagamiya, H.Bowman, J.Ioannou, and J.O.Rasmussen, Proceedings of Internat'l Conf. on Nuclear Structure, Tokyo, Japan (Sept. 5-10, 1977).

10. S.Nagamiya, I.Tanihata, S.Schnetzer, A.Anderson, W.Brückner, O.Chamberlain, G.Shapiro, H.Steiner, Proceedings of Internat'l Conf. on Nuclear Structure, Tokyo, Japan (Sept. 5-10, 1977); also LBL-6770.

11. J.Gosset, H.H.Gutbrod, Ch.King, G.King, Ch.Lukner, W.G.Meyer, Nguyen,V.S., A.M.Poskanzer, A.Sandoval, R.Stock, G.D.Westfall, and K.Wolff, to be published.

12. S.T.Butler, C.A.Pearson, Phys. Rev. Lett. 7, 69 (1961); A.Schwarzschild, Č.Zupančič, Phys. Rev. 129, 854 (1963).

13. H.H.Gutbrod, A.Sandoval, P.J.Johansen, A.M.Poskanzer, J.Gosset, W.G.Meyer, G.D.Westfall, and R.Stock, Phys. Rev. Lett. 37, 667 (1976).

14. W.G.Meyer, H.H.Gutbrod, Ch.Lukner, and A.Sandoval, to be published.

15. A.M.Poskanzer, G.W.Butler, and E.K.Hyde, Phys. Rev. C3, 882 (1971).

16. R.Hagedorn, 1973 Cargèse Lectures in Physics, E.Schatzmann editor (Gordon & Breach, New York) Vol. 6, p.643.

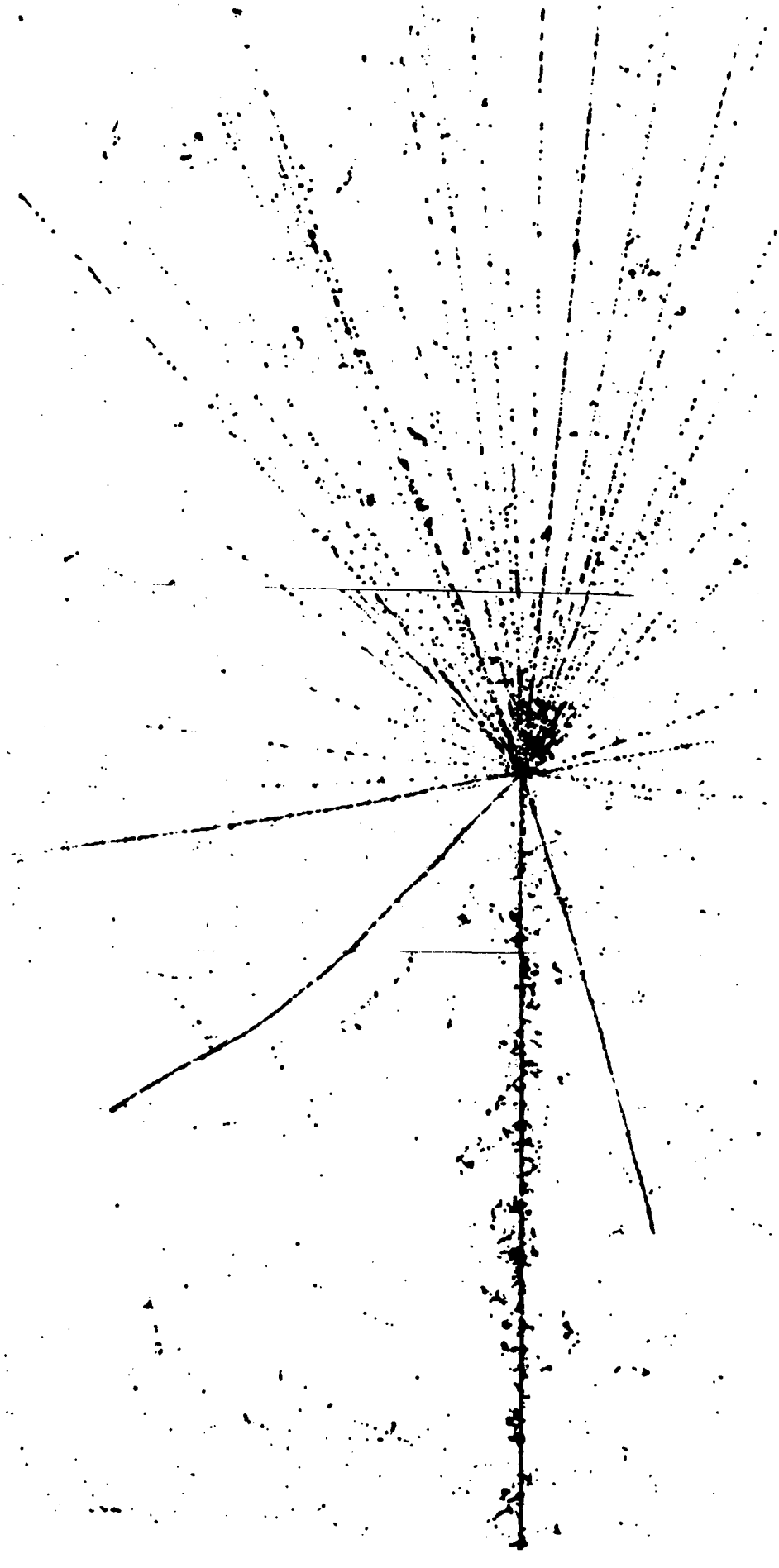

XBB 771-31

Fig. 1 1.8 GeV/n ^{40}Ar + emulsion
Heckmann et al.

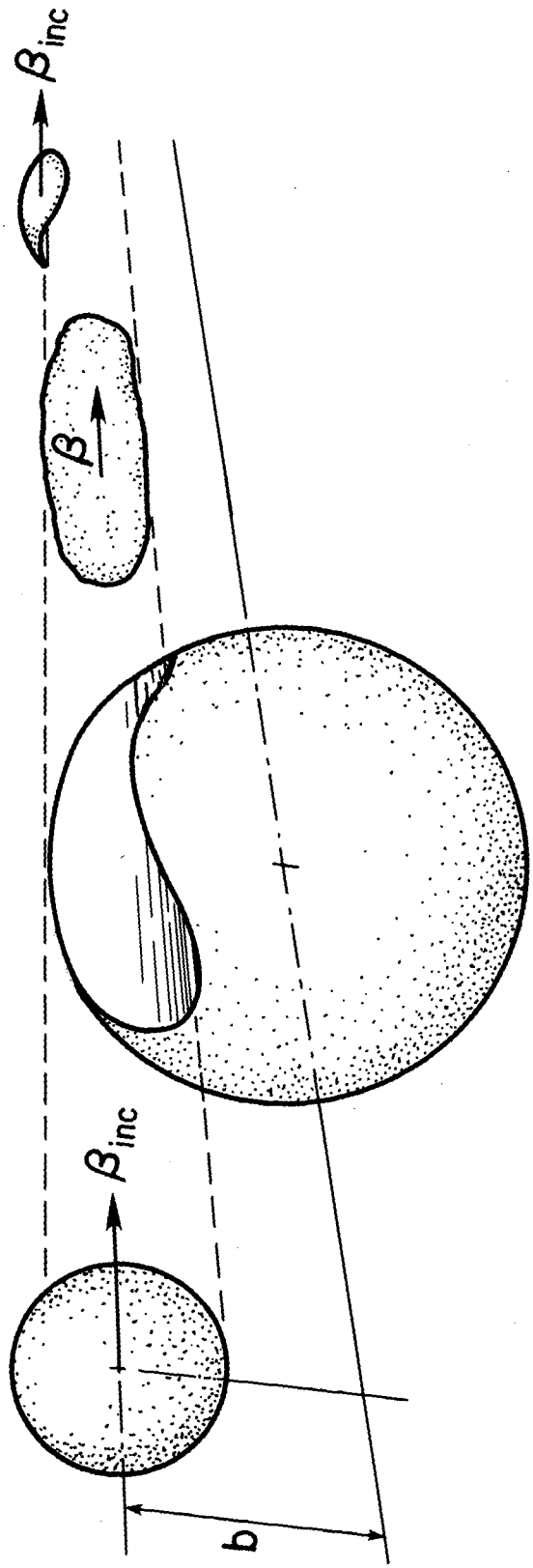

XBL 768-3876

Fig. 2

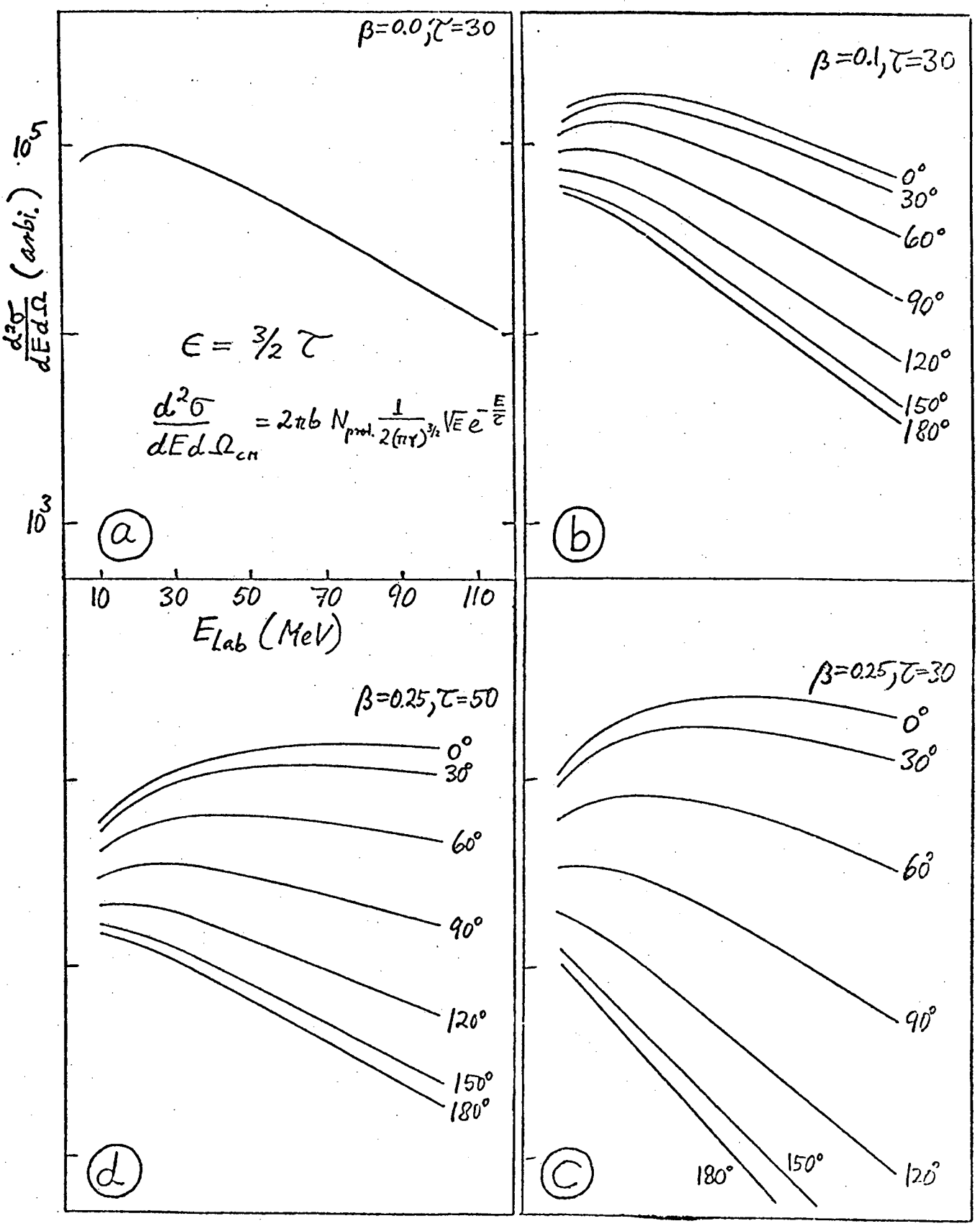
β=0.0, τ=30
β=0.1, τ=30
β=0.25, τ=50
β=0.25, τ=30
$\frac{d^2\sigma}{dE d\Omega}$ (arbi.)
10^5
10^3
$\epsilon = 3/2\ \tau$
$\frac{d^2\sigma}{dE d\Omega_{cm}} = 2\pi b\, N_{prod.} \frac{1}{2(\pi\tau)^{3/2}} \sqrt{E}\, e^{-\frac{E}{\tau}}$
10 30 50 70 90 110
E_{Lab} (MeV)
0°
30°
60°
90°
120°
150°
180°
a
b
c
d

Fig. 3.

$^{20}Ne \rightarrow {}^{238}U$ at 250 MeV/n

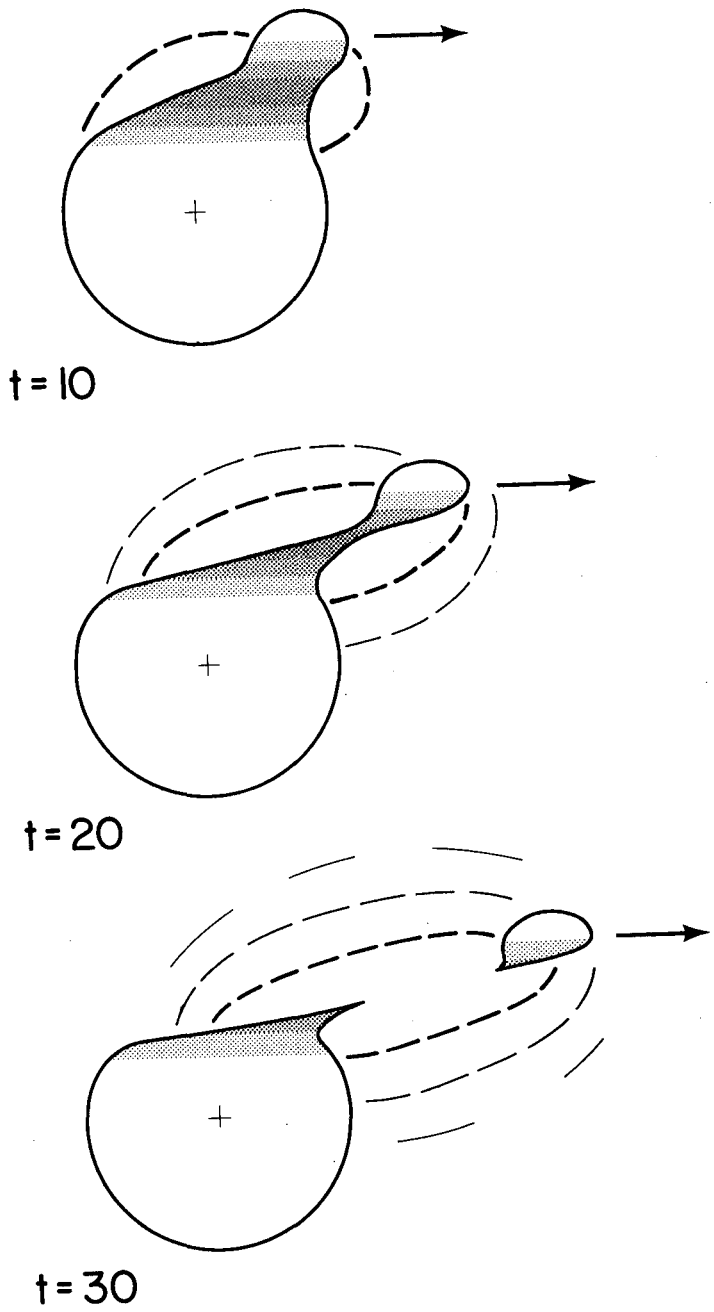

XBL 778-1680

Fig. 4

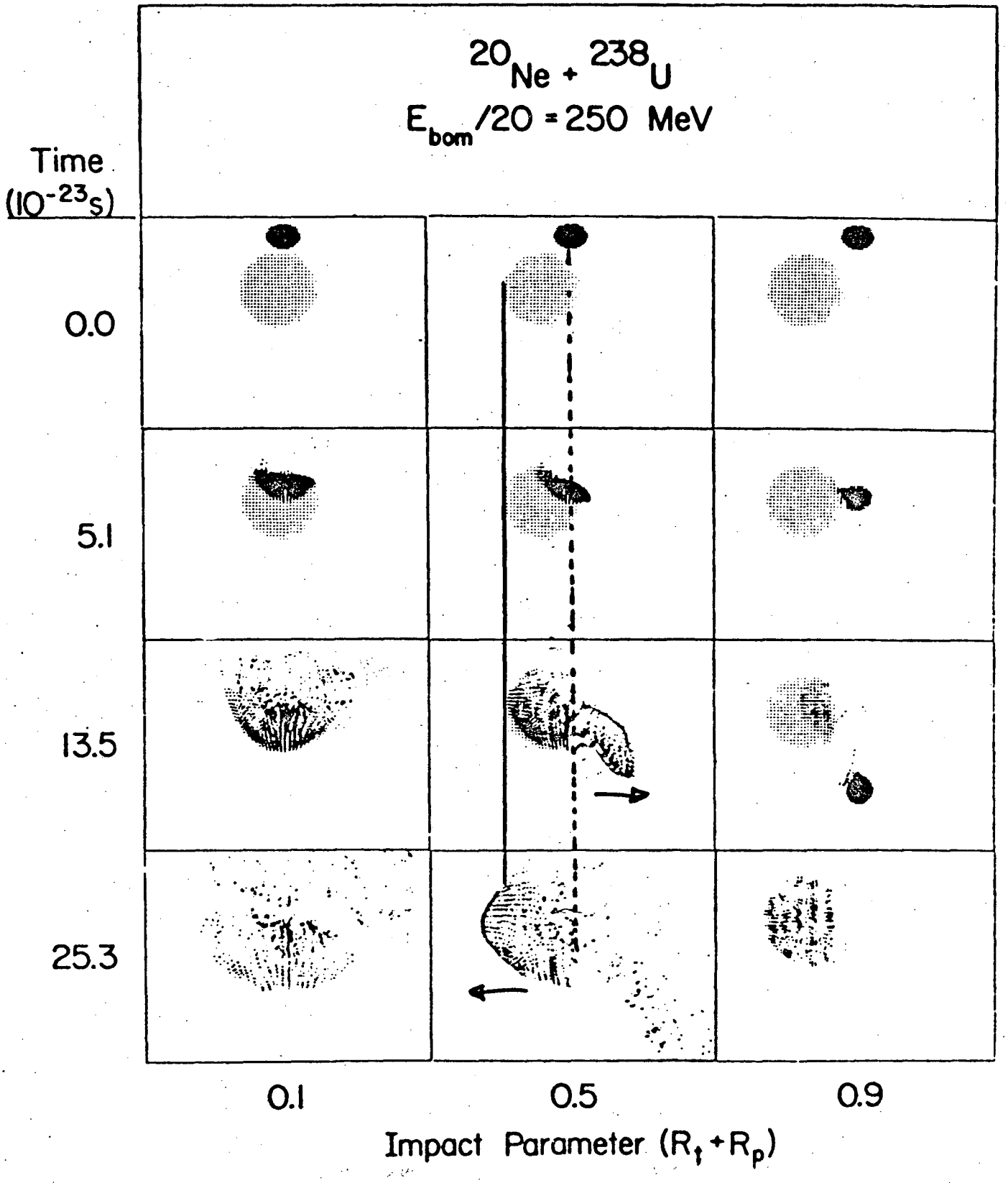
$^{20}Ne + ^{238}U$
$E_{bom}/20 = 250$ MeV
Time
$(10^{-23}s)$
0.0
5.1
13.5
25.3
0.1
0.5
0.9
Impact Parameter $(R_t + R_p)$

Fig. 5

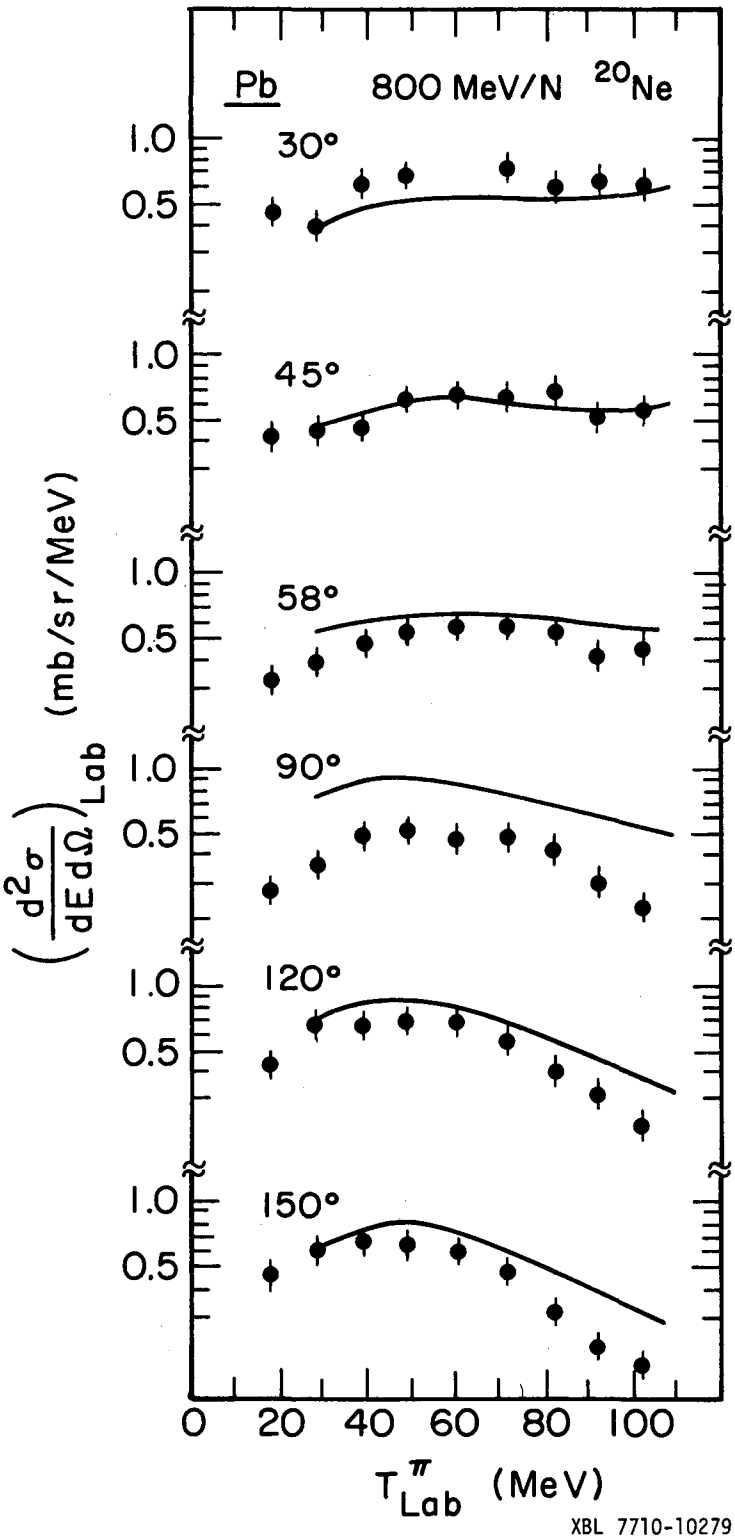
Pb
800 MeV/N ^{20}Ne
30°
45°
58°
90°
120°
150°
1.0
0.5
0
20
40
60
80
100
$\left(\frac{d^2\sigma}{dE\,d\Omega}\right)_{Lab}$ (mb/sr/MeV)
T^{π}_{Lab} (MeV)
XBL 7710-10279

Fig. 6

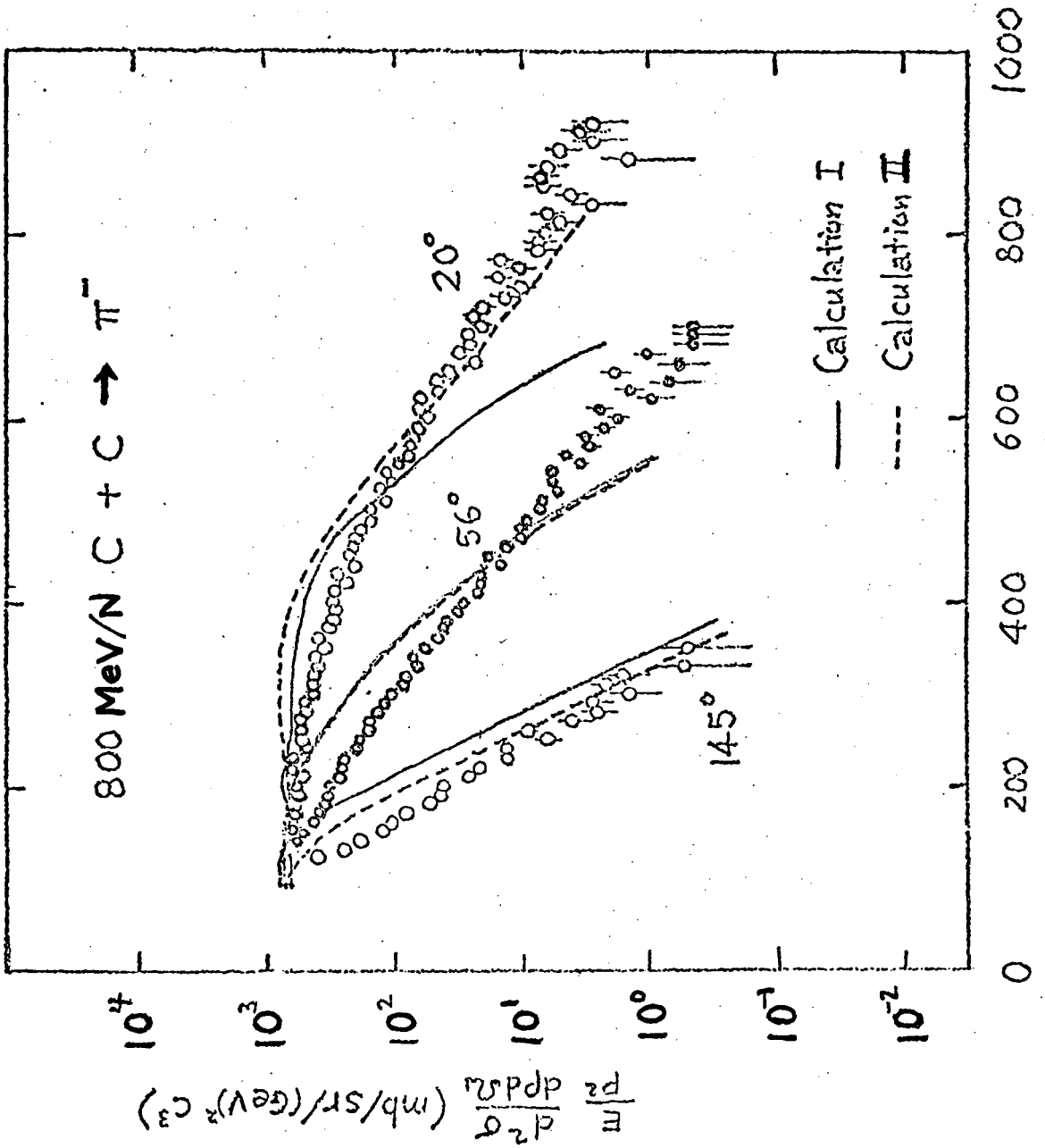
800 MeV/N C + C → π⁻
20°
56°
145°
Calculation I
Calculation II
$\frac{E}{p^2}\frac{d^2\sigma}{dpd\Omega}$ (mb/sr/(GeV)² c³)
MOMENTUM (MeV/c)
0
200
400
600
800
1000
10^{4}
10^{3}
10^{2}
10^{1}
10^{0}
10^{-1}
10^{-2}

Fig 7

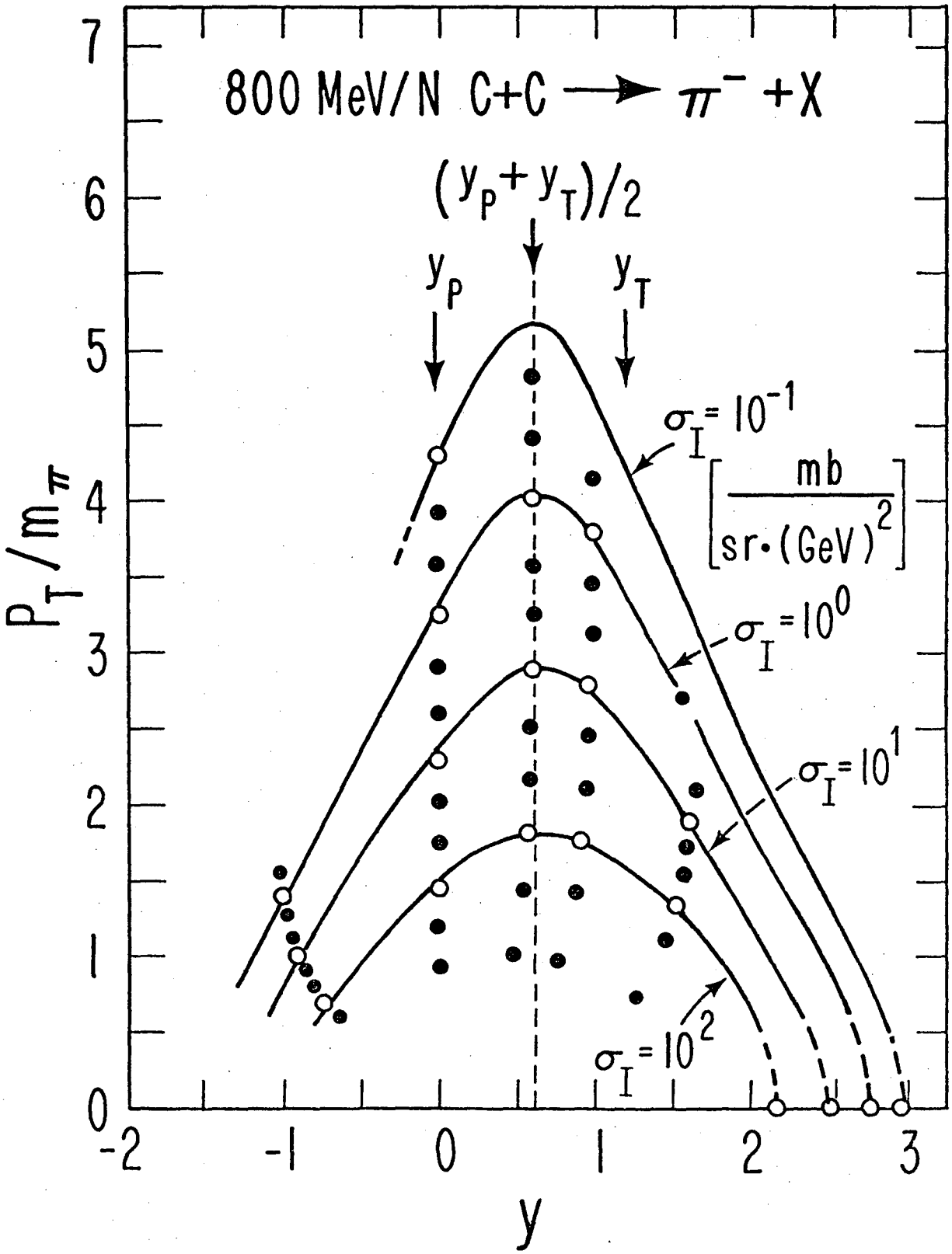

XBL779-1893

Fig 8

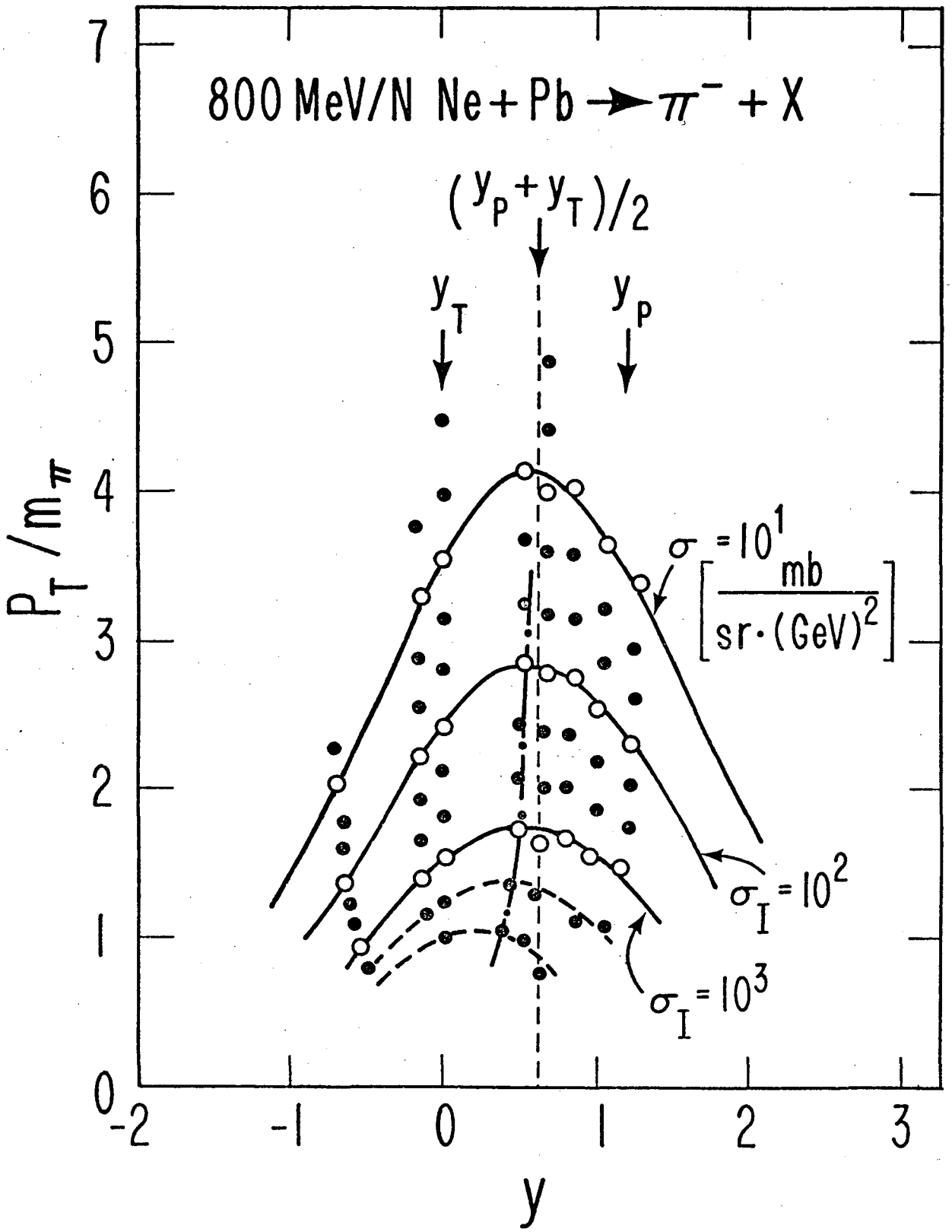

XBL 779-1891

Fig 9

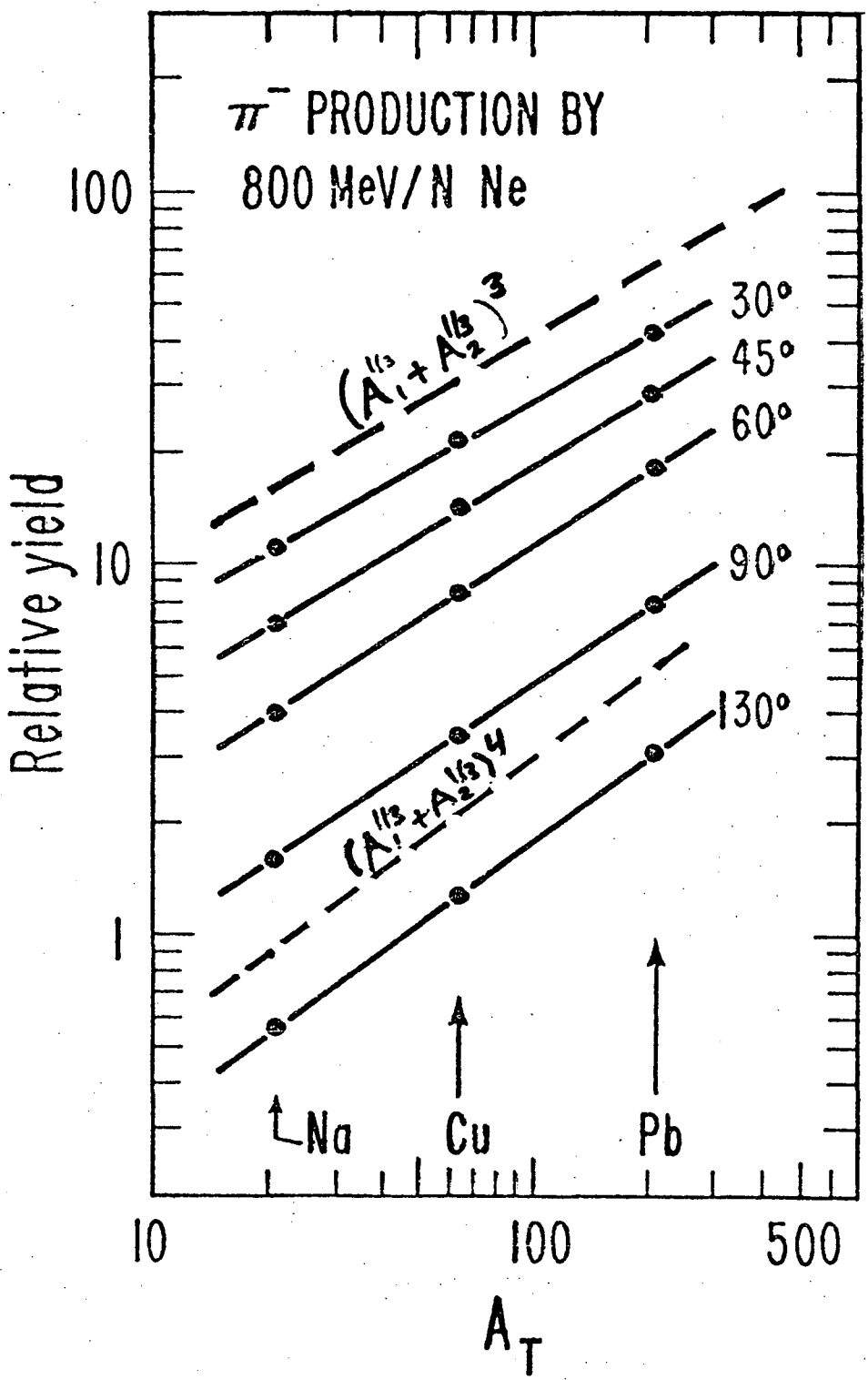
π^- PRODUCTION BY
800 MeV/N Ne
100
10
1
Relative yield
$(A_1^{1/3}+A_2^{1/3})^3$
$(A_1^{1/3}+A_2^{1/3})^4$
30°
45°
60°
90°
130°
Na
Cu
Pb
10
100
500
A_T

Fig 10

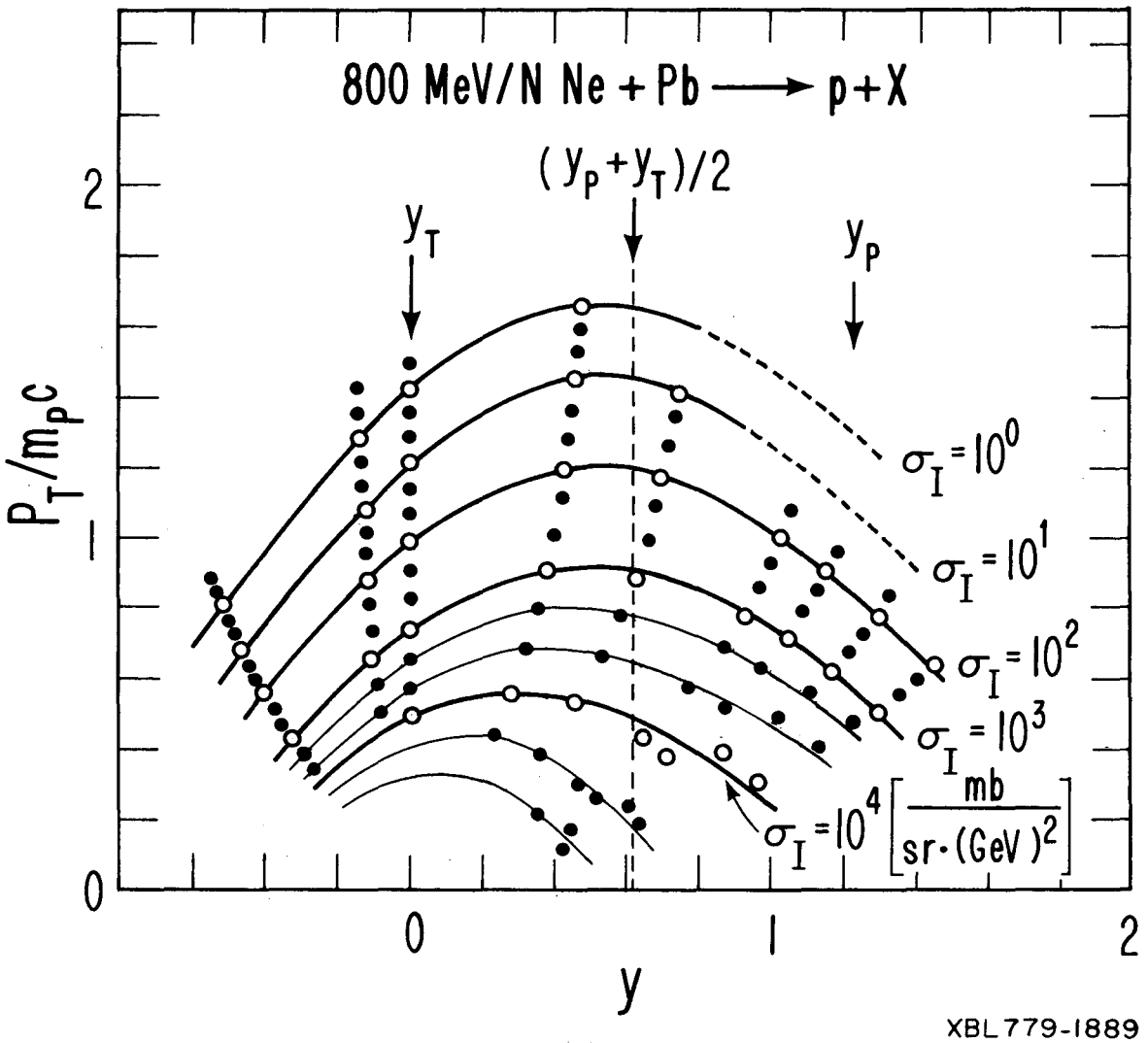
800 MeV/N Ne + Pb ⟶ p+X
$(y_p+y_T)/2$
y_T
y_p
$\sigma_I = 10^0$
$\sigma_I = 10^1$
$\sigma_I = 10^2$
$\sigma_I = 10^3$
$\sigma_I = 10^4 \left[\frac{mb}{sr\cdot(GeV)^2}\right]$
P_T/m_pc
y
0
1
2
XBL779-1889

Fig. 11

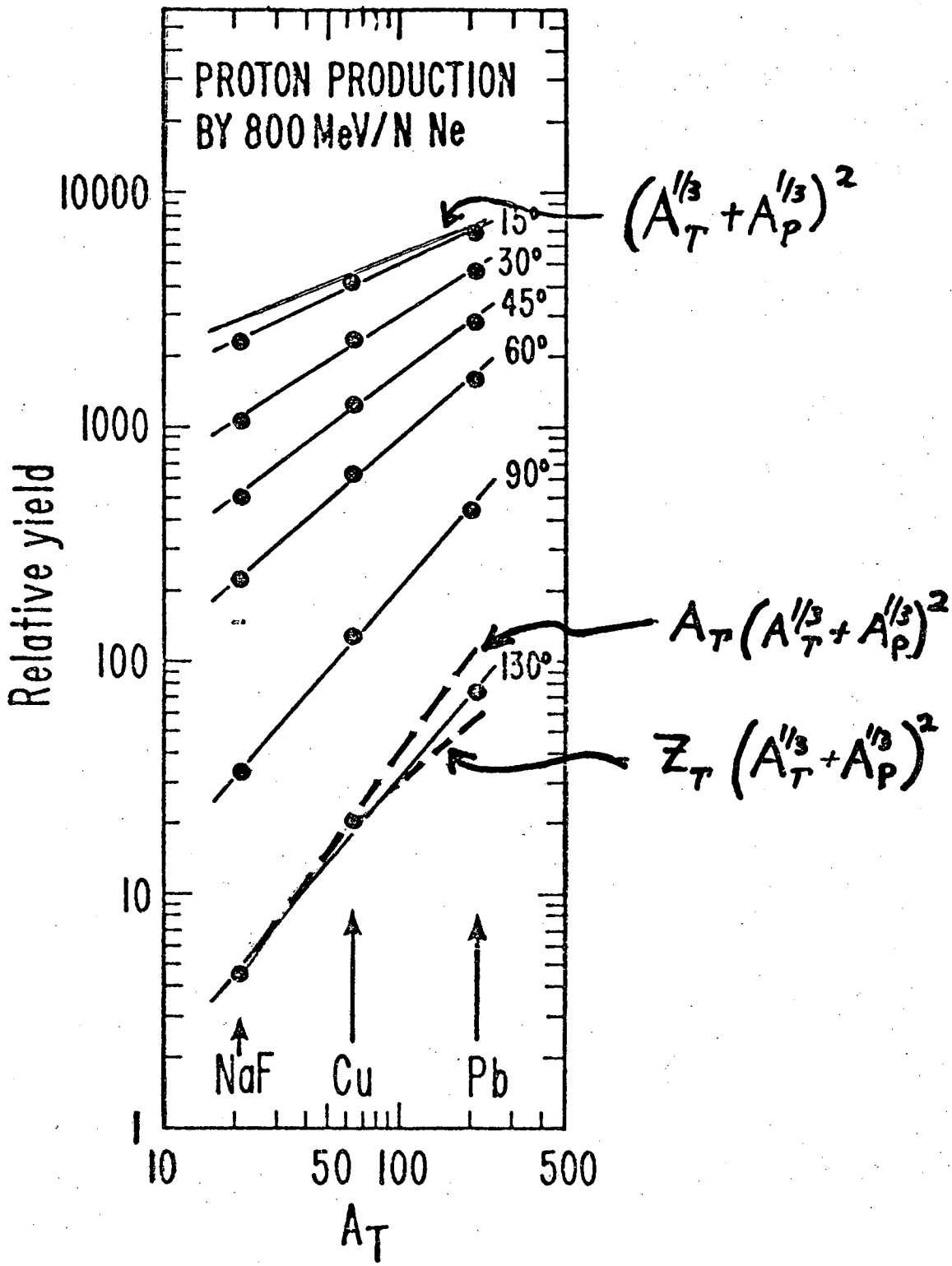
PROTON PRODUCTION
BY 800 MeV/N Ne
Relative yield
10000
1000
100
10
1
15°
30°
45°
60°
90°
130°
$(A_T^{1/3} + A_P^{1/3})^2$
$A_T(A_T^{1/3} + A_P^{1/3})^2$
$Z_T(A_T^{1/3} + A_P^{1/3})^2$
NaF
Cu
Pb
10
50
100
500
A_T

Fig. 12

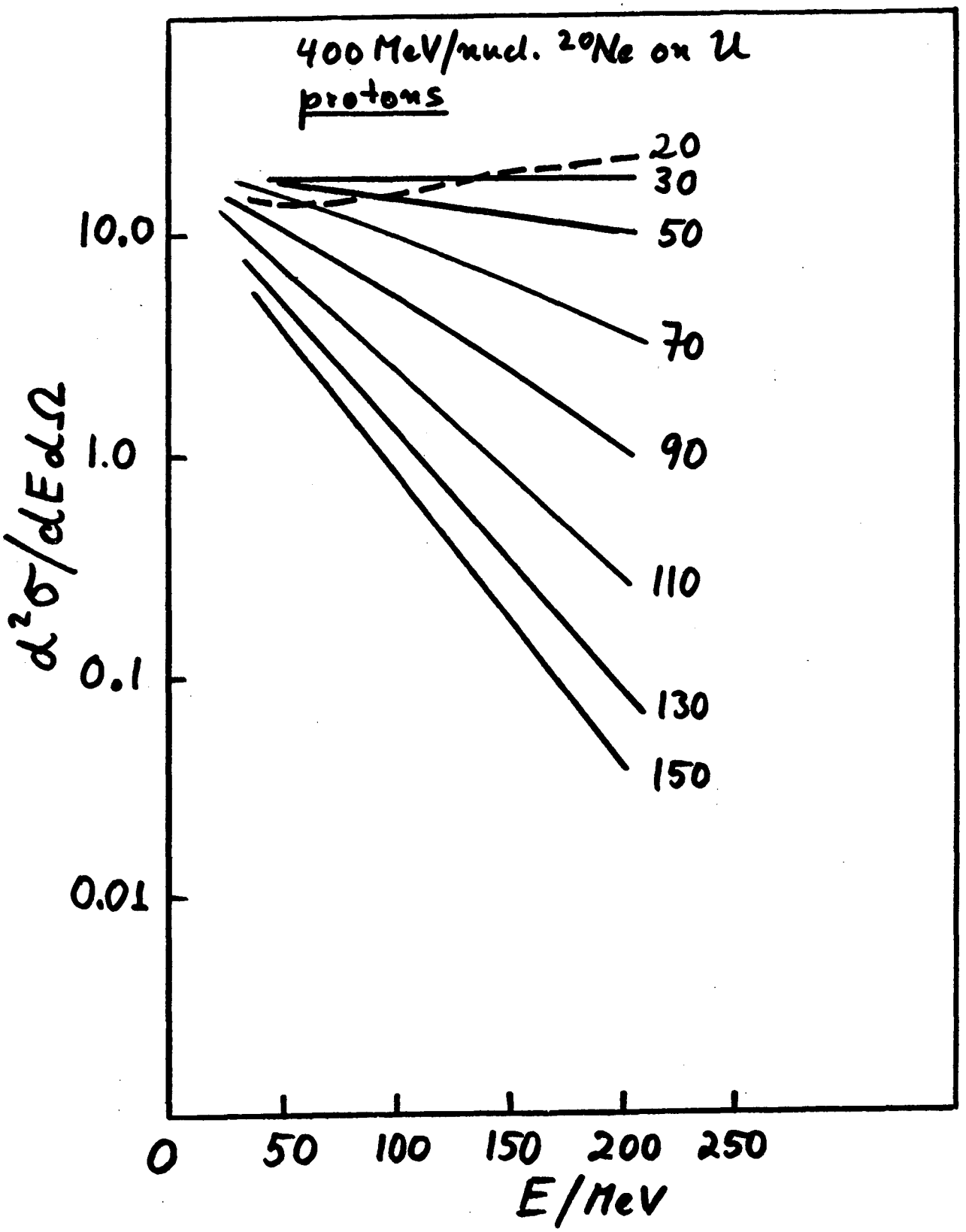
400 MeV/nucl. ^{20}Ne on U
protons
20
30
50
70
90
110
130
150
10.0
1.0
0.1
0.01
$d^2\sigma/dE d\Omega$
0
50
100
150
200
250
E/MeV

Fig 13

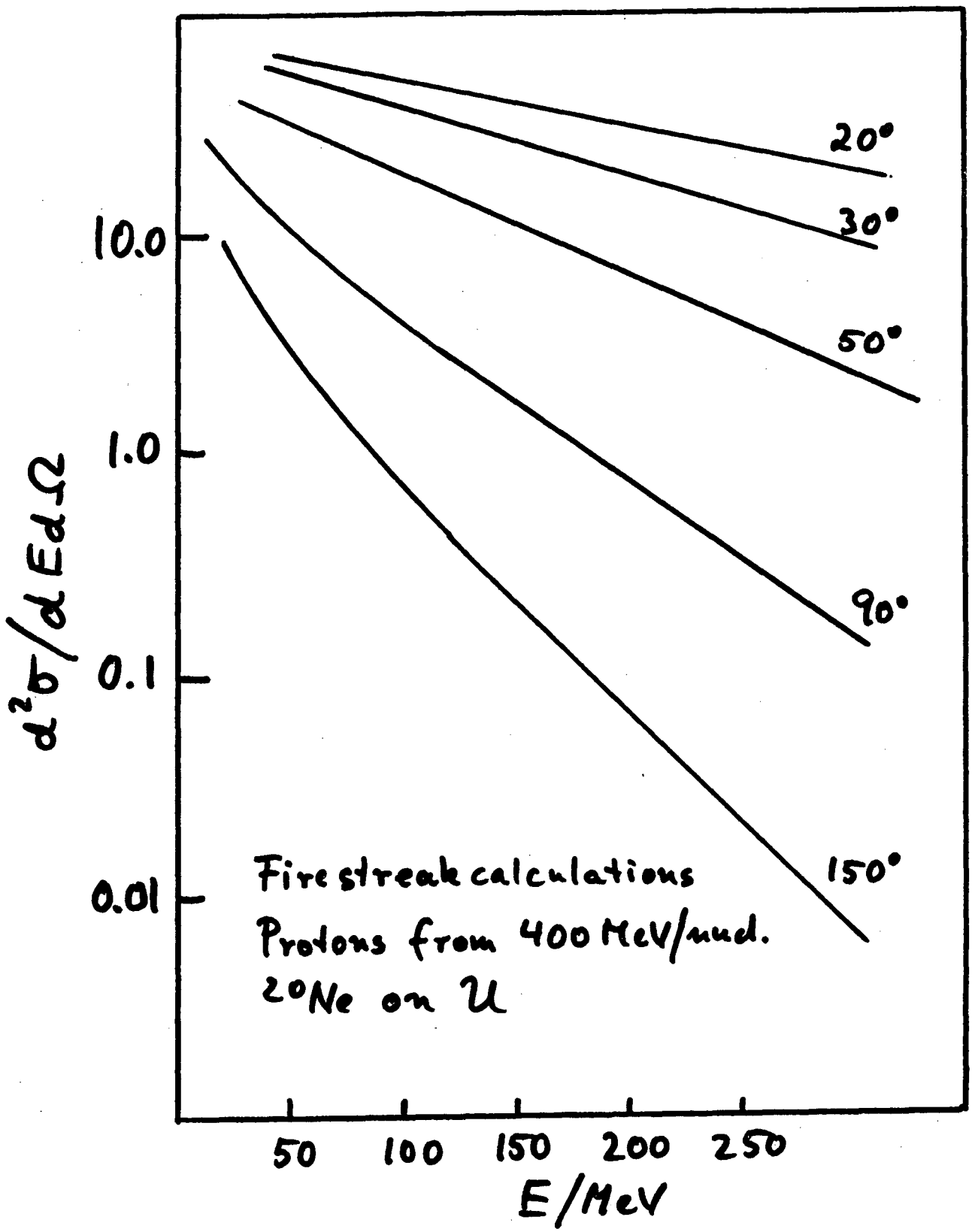
20°
30°
50°
90°
150°
10.0
1.0
0.1
0.01
$d^2\sigma/dEd\Omega$
Fire streak calculations
Protons from 400 MeV/nucl.
^{20}Ne on U
50
100
150
200
250
E/MeV

Fig 14

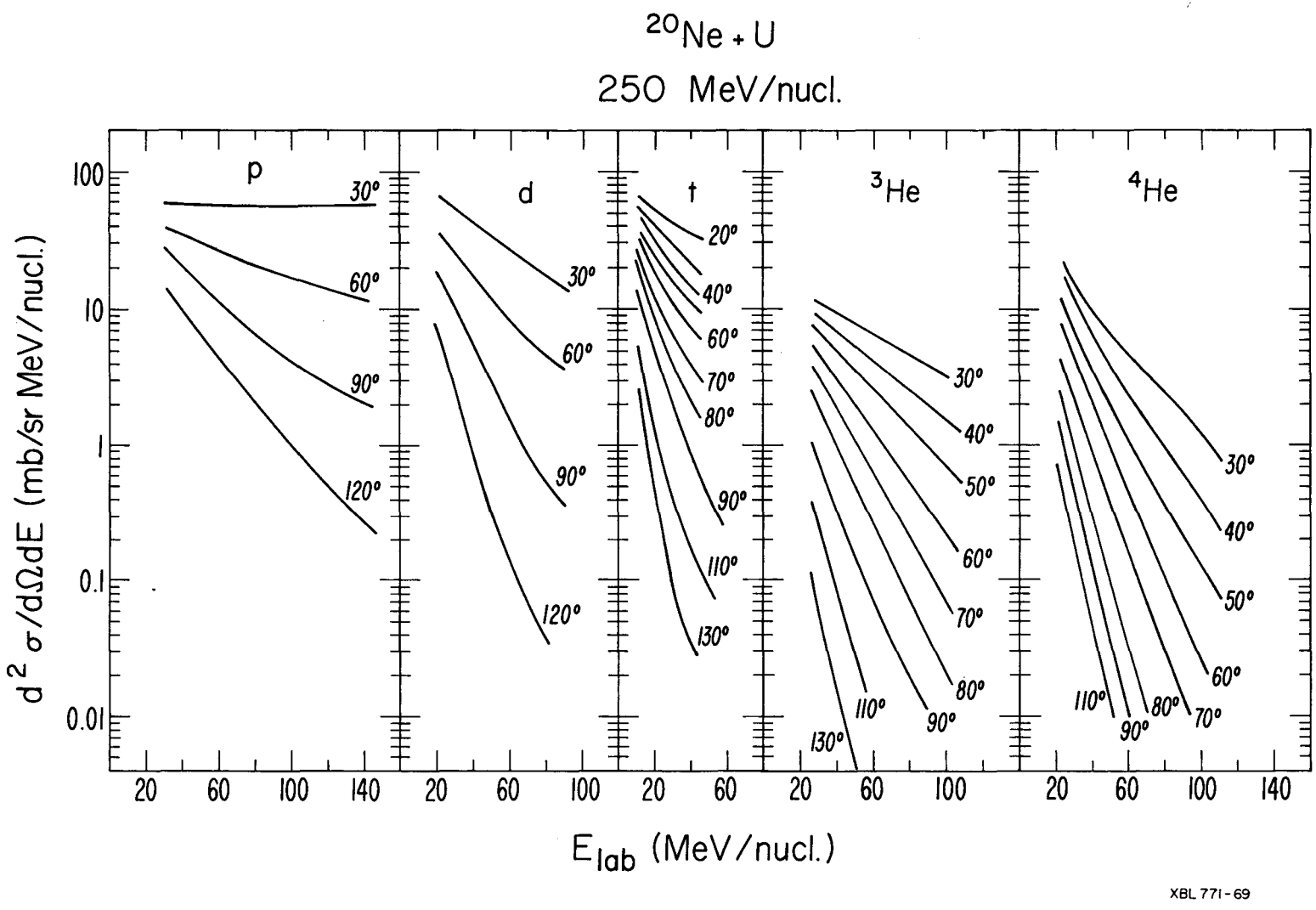

XBL 771-69

Fig. 15

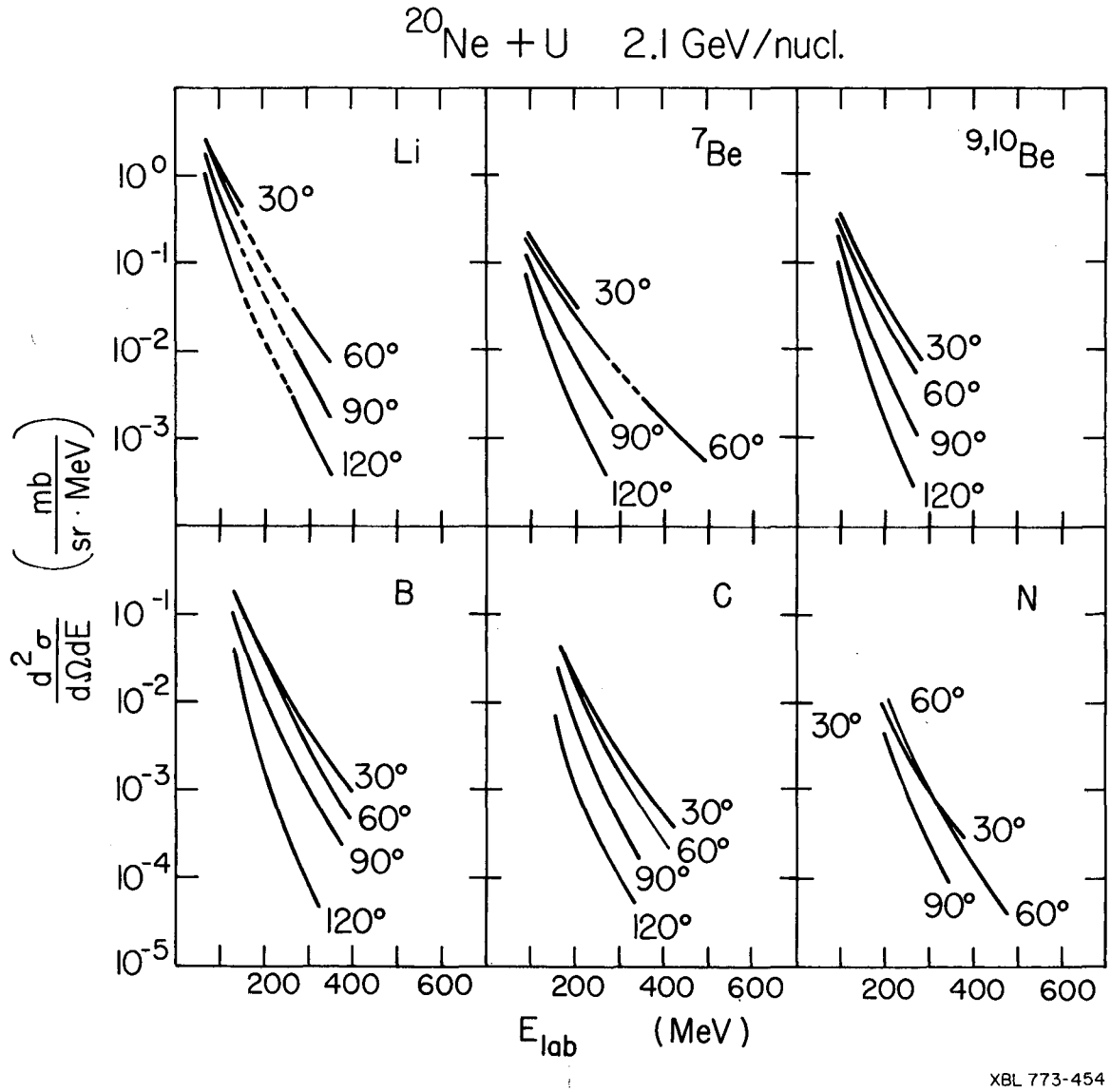
^{20}Ne + U 2.1 GeV/nucl.
Li
^{7}Be
^{9,10}Be
B
C
N
30°
60°
90°
120°
$\frac{d^2\sigma}{d\Omega dE}$ $\left(\frac{mb}{sr \cdot MeV}\right)$
10^{0}
10^{-1}
10^{-2}
10^{-3}
10^{-4}
10^{-5}
200 400 600
E_{lab} (MeV)
XBL 773-454

Fig. 16

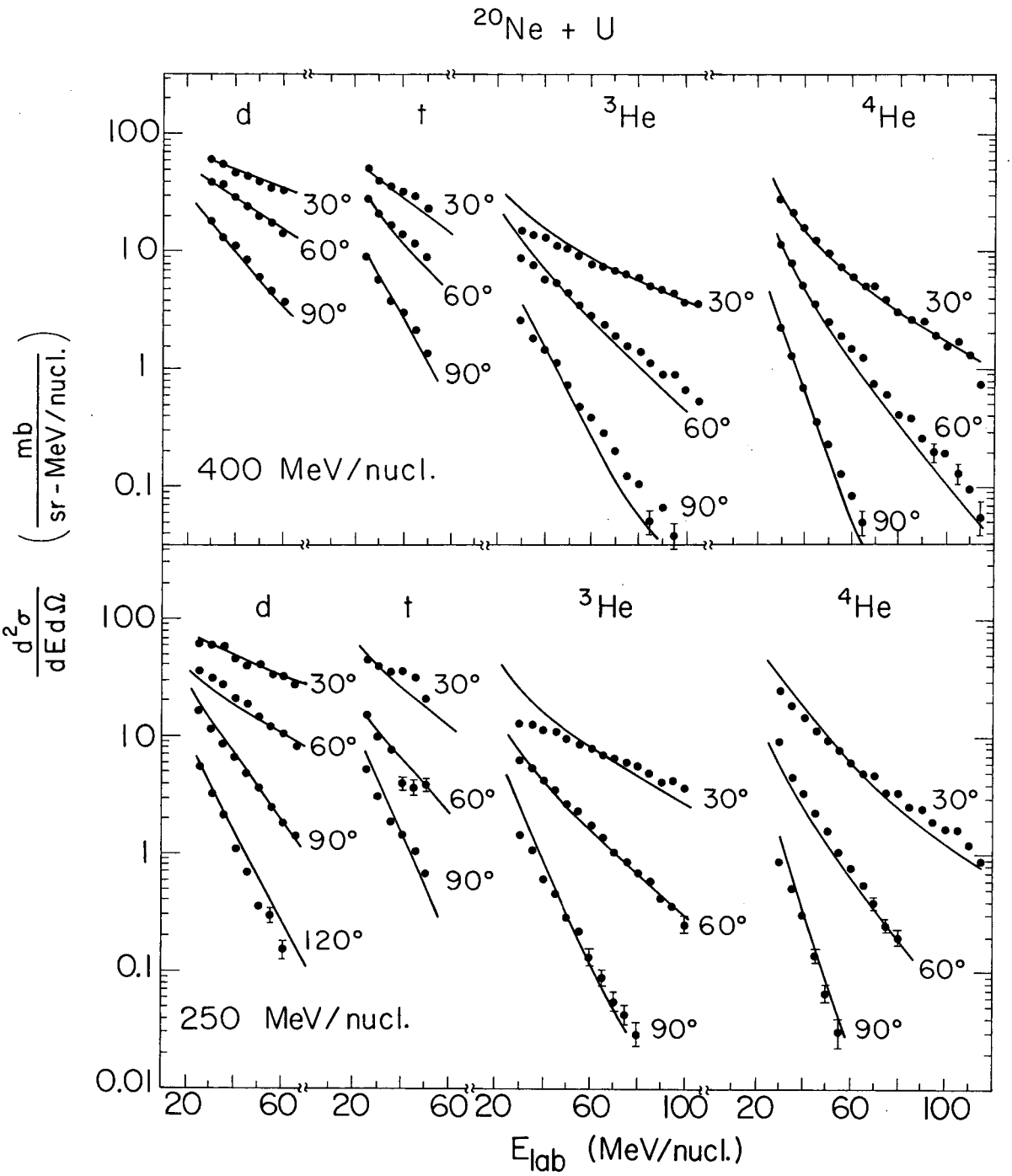
^{20}Ne + U
d
t
^{3}He
^{4}He
400 MeV/nucl.
250 MeV/nucl.
30°
60°
90°
120°
100
10
1
0.1
0.01
20
60
100
E_{lab} (MeV/nucl.)
$\frac{d^2\sigma}{dE\,d\Omega}$ $\left(\frac{mb}{sr\text{-}MeV/nucl.}\right)$
XBL767-3109

Fig. 17

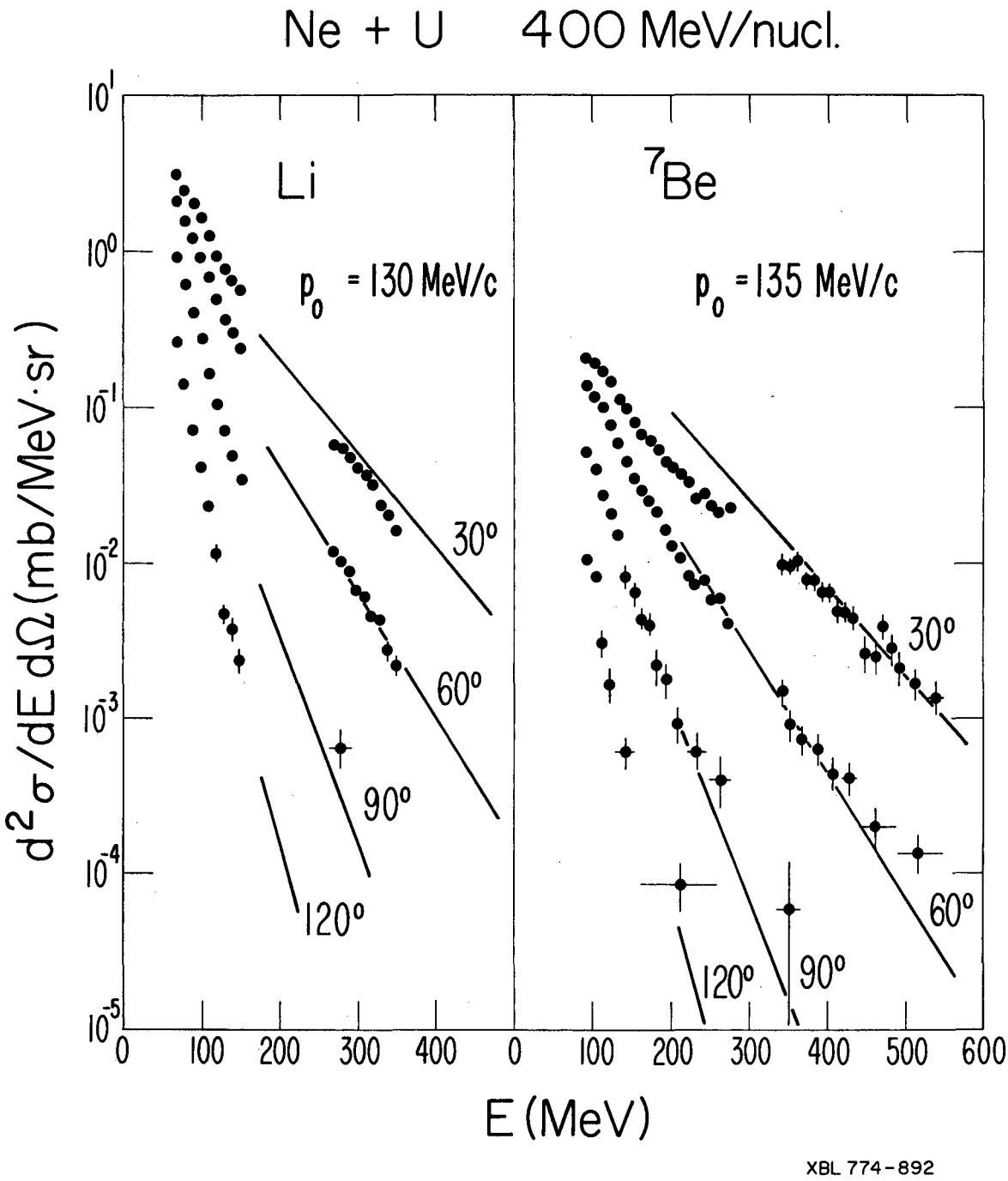
Ne + U 400 MeV/nucl.
Li
^{7}Be
p_0 = 130 MeV/c
p_0 = 135 MeV/c
30°
60°
90°
120°
$d^2\sigma/dE\,d\Omega$ (mb/MeV·sr)
E (MeV)
XBL 774-892

Fig. 18

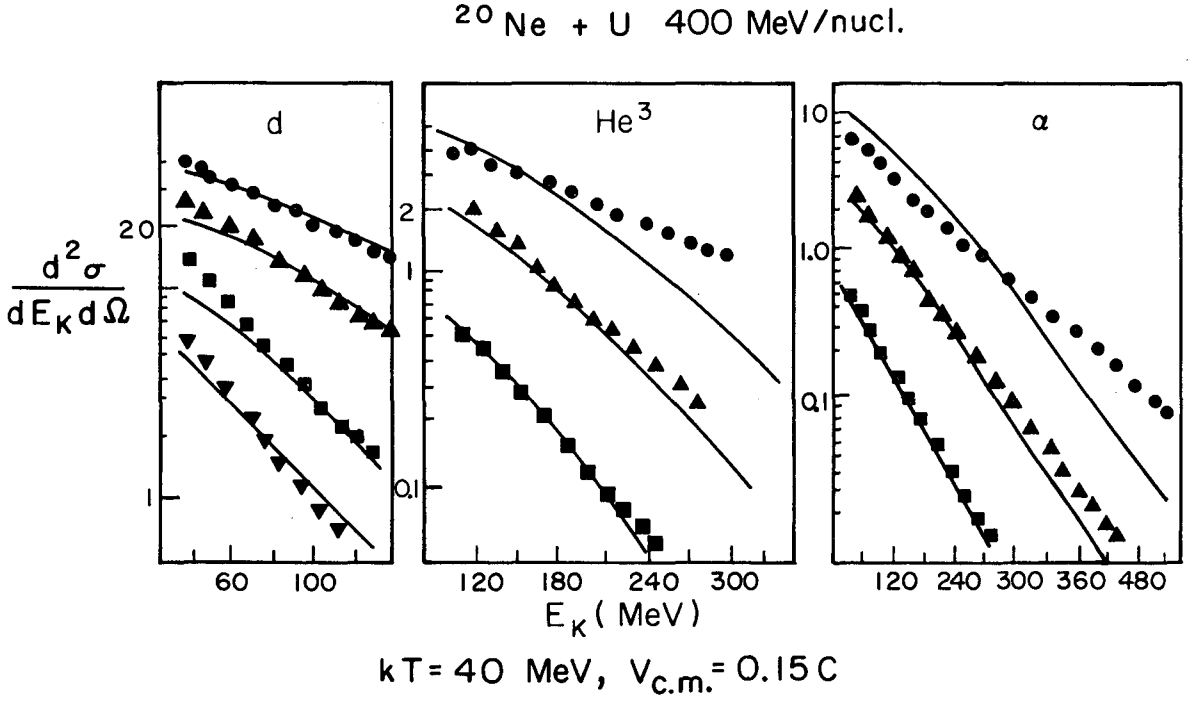
^{20}Ne + U 400 MeV/nucl.
d
He^3
α
$\frac{d^2\sigma}{dE_K d\Omega}$
20
1
2
1
0.1
10
1.0
0.1
60
100
120
180
240
300
120
240
300
360
480
E_K (MeV)
kT = 40 MeV, $V_{c.m.}$ = 0.15 C
XBL776-1281

Fig. 19

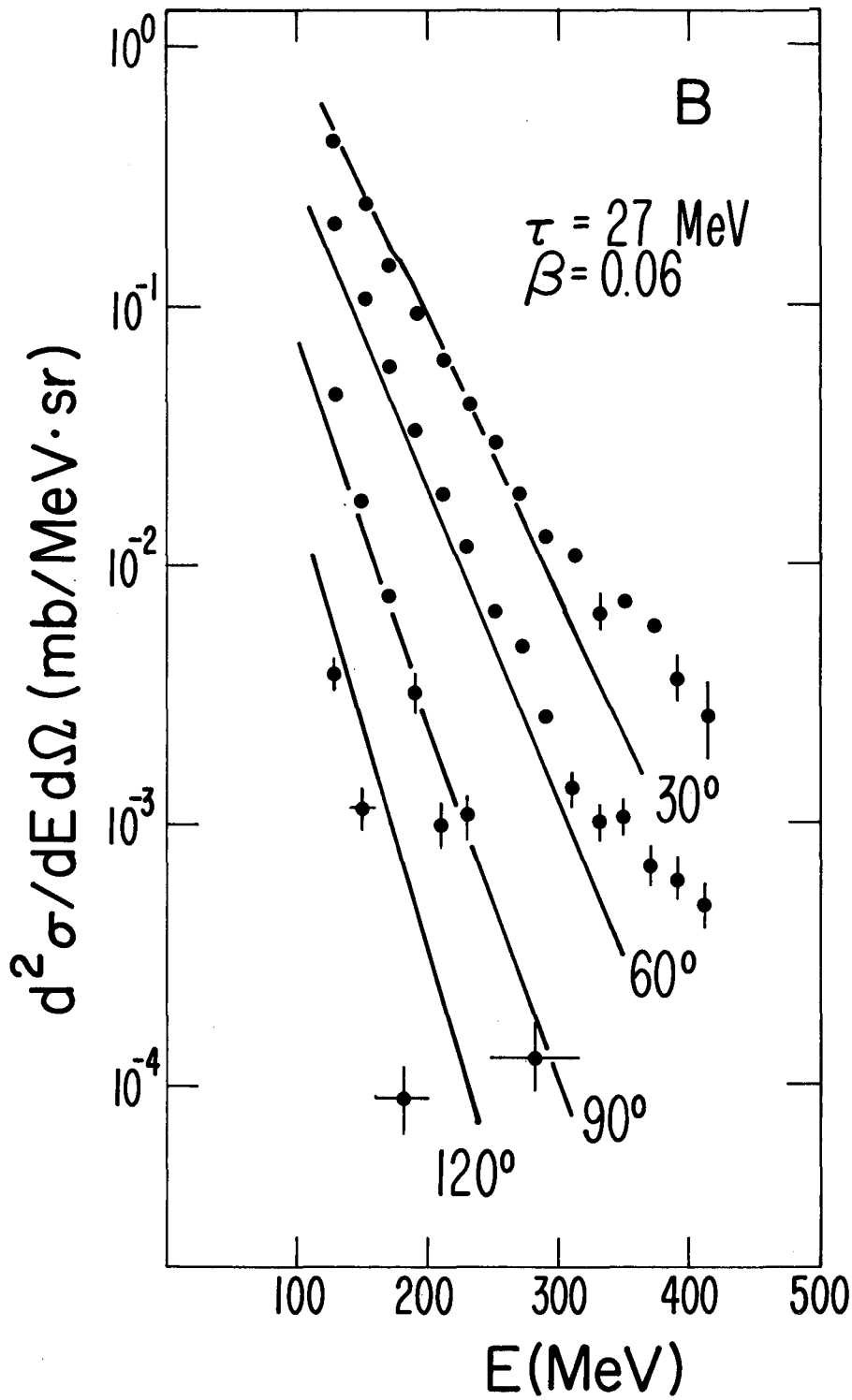

XBL 774-891

Fig. 20

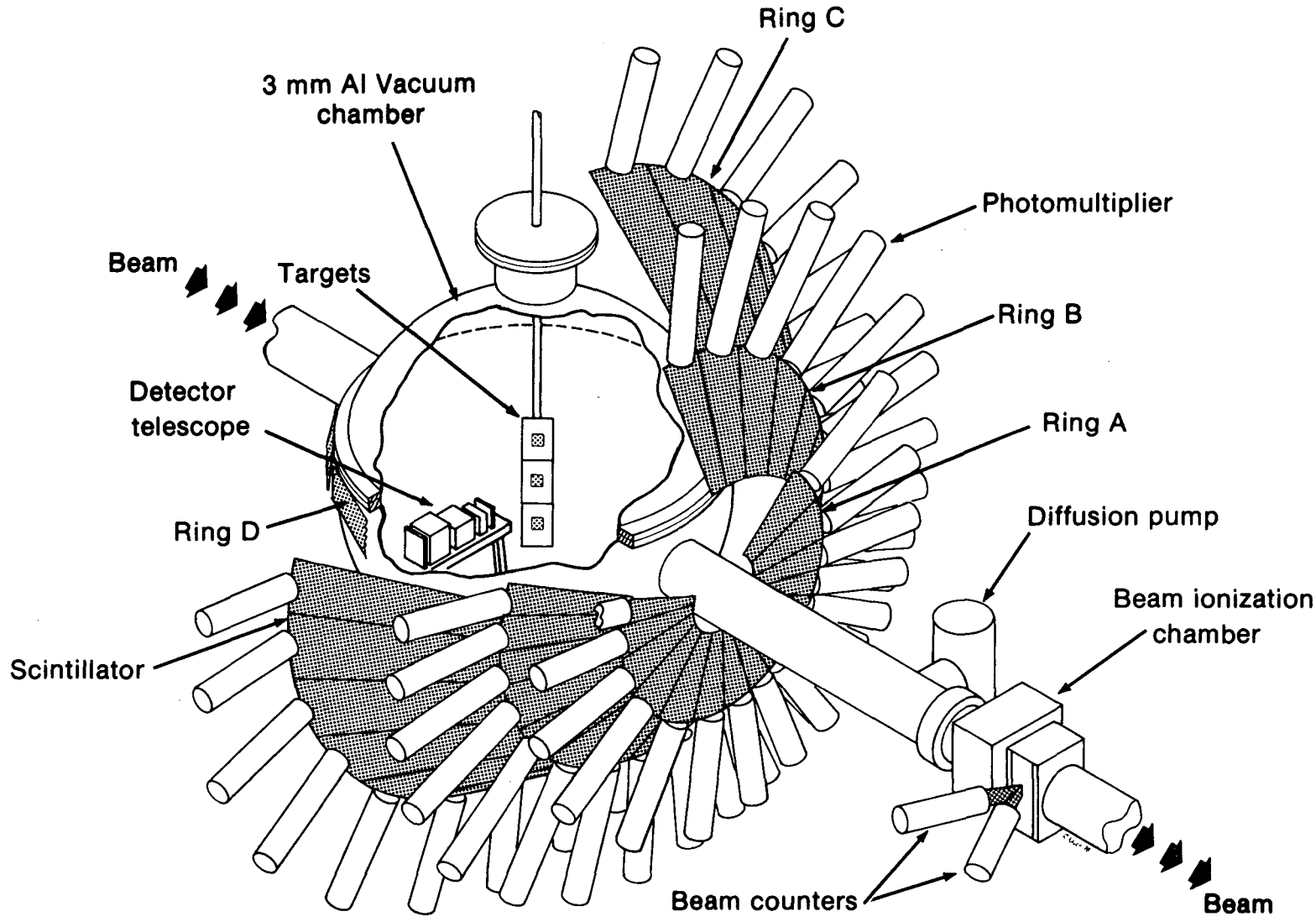
Ring C
3 mm Al Vacuum chamber
Photomultiplier
Beam
Targets
Ring B
Detector telescope
Ring A
Ring D
Diffusion pump
Beam ionization chamber
Scintillator
Beam counters
Beam
XBL 782-7229C

Fig. 21

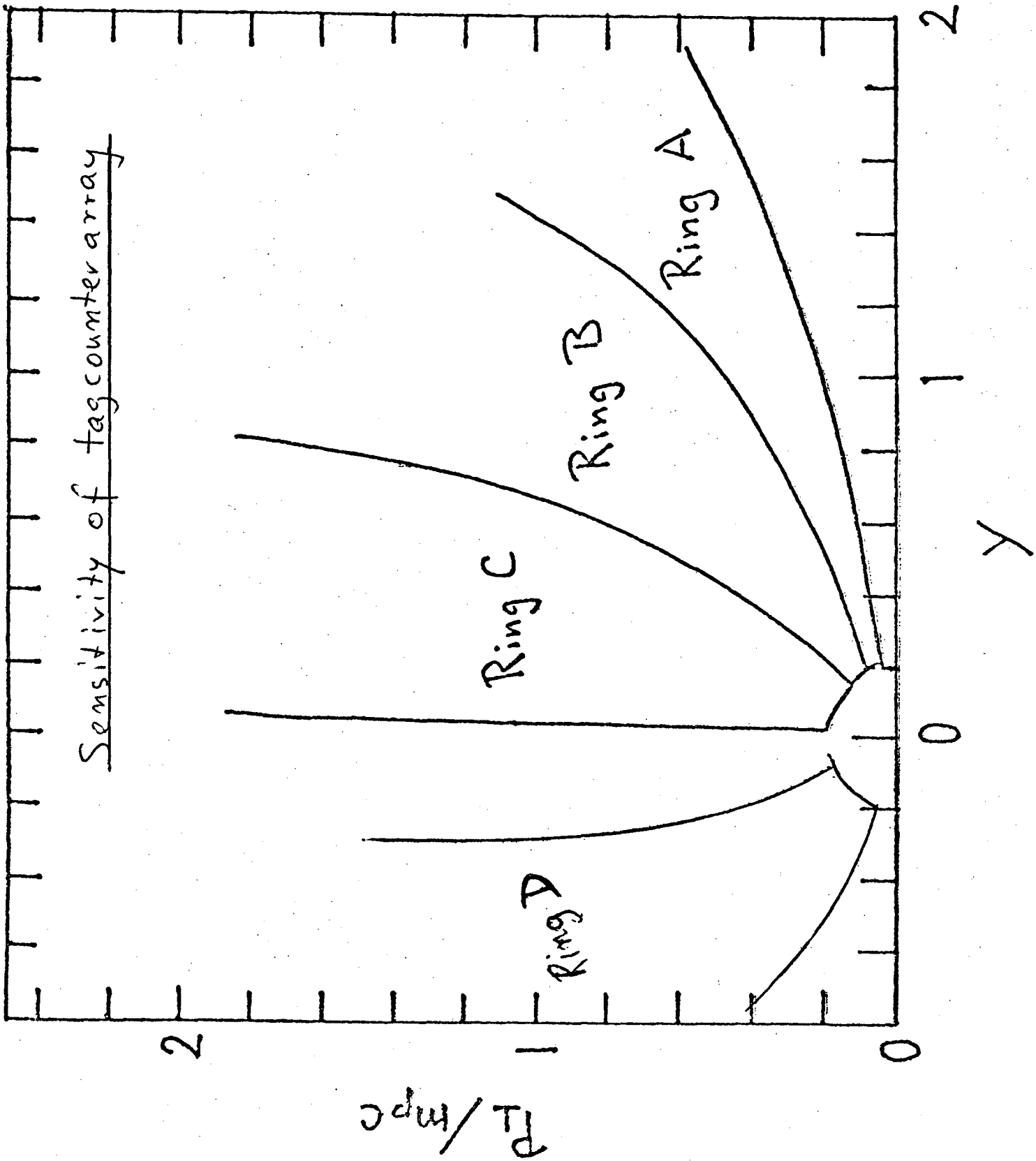
Sensitivity of tag counter array
Ring A
Ring B
Ring C
Ring D
P_L/mpc
0
1
2
Y

Fig 22

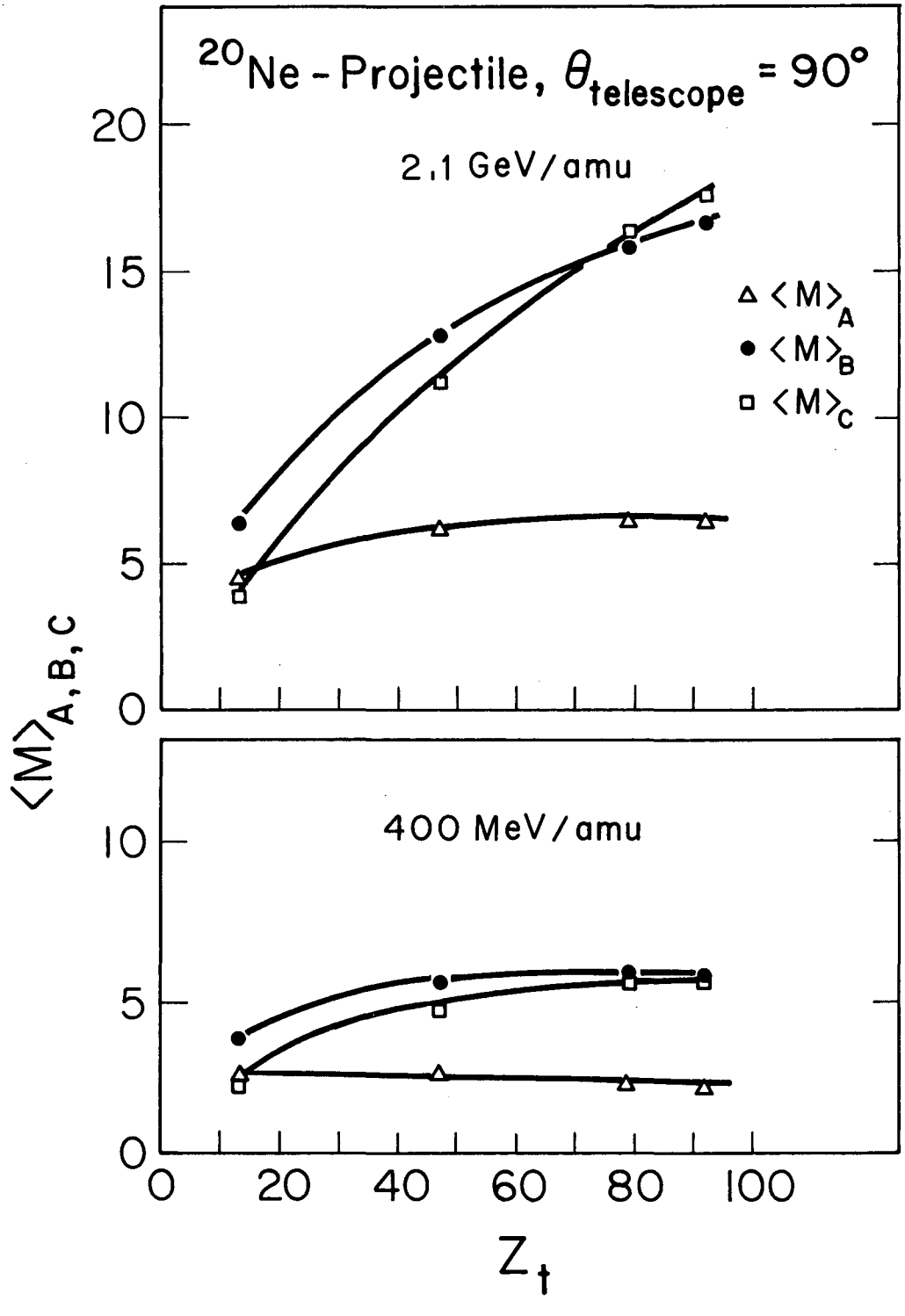

XBL 782-244

Fig. 23

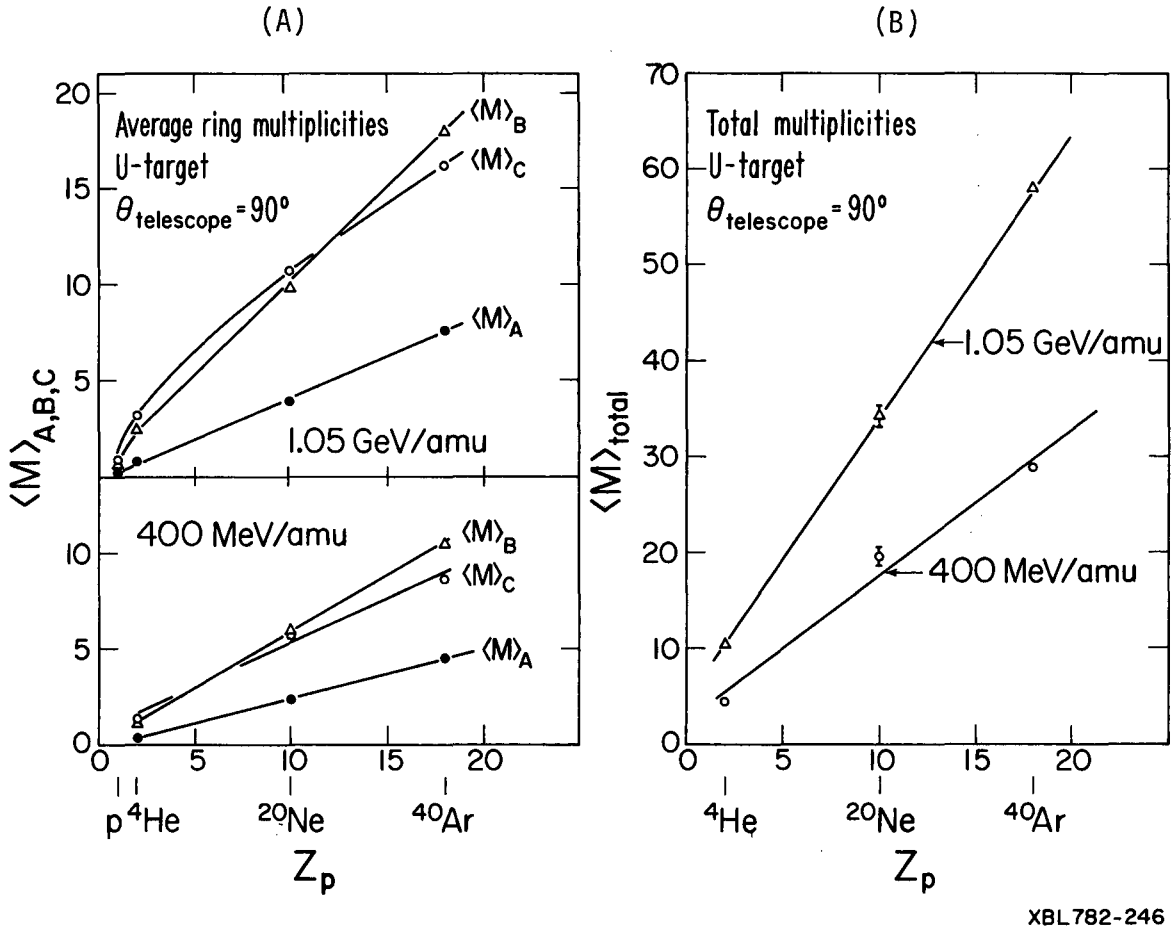
(A)
(B)
Average ring multiplicities
U-target
$\theta_{telescope} = 90°$
$\langle M \rangle_B$
$\langle M \rangle_C$
$\langle M \rangle_A$
1.05 GeV/amu
400 MeV/amu
$\langle M \rangle_{A,B,C}$
Total multiplicities
U-target
$\theta_{telescope} = 90°$
1.05 GeV/amu
400 MeV/amu
$\langle M \rangle_{total}$
p
^{4}He
^{20}Ne
^{40}Ar
Z_p
XBL782-246

Fig. 24

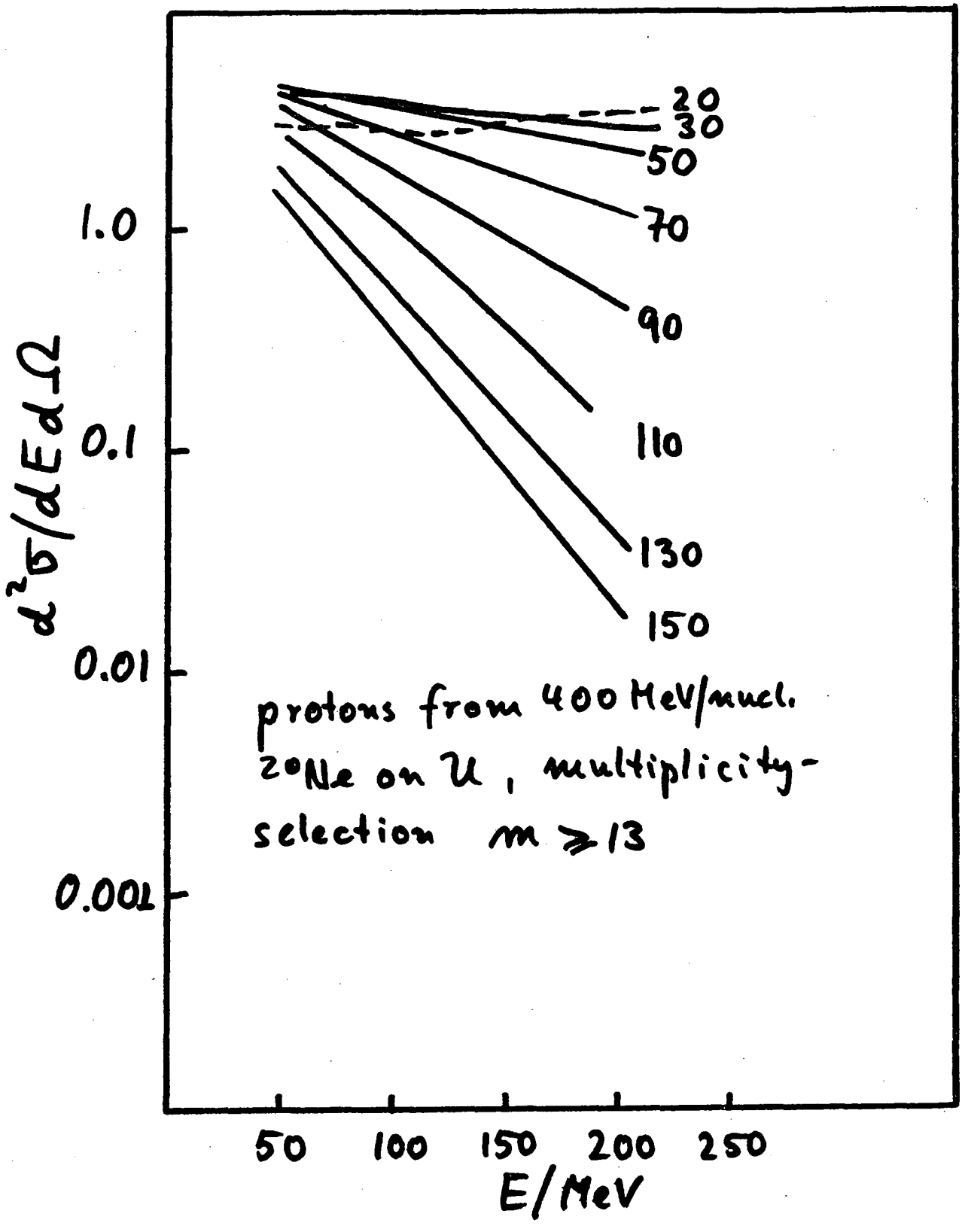
20
30
50
70
90
110
130
150
1.0
0.1
0.01
0.001
$d^2\sigma/dE\,d\Omega$
protons from 400 MeV/nucl.
^{20}Ne on U, multiplicity-
selection $m \geq 13$
50
100
150
200
250
E/MeV

Fig 25a

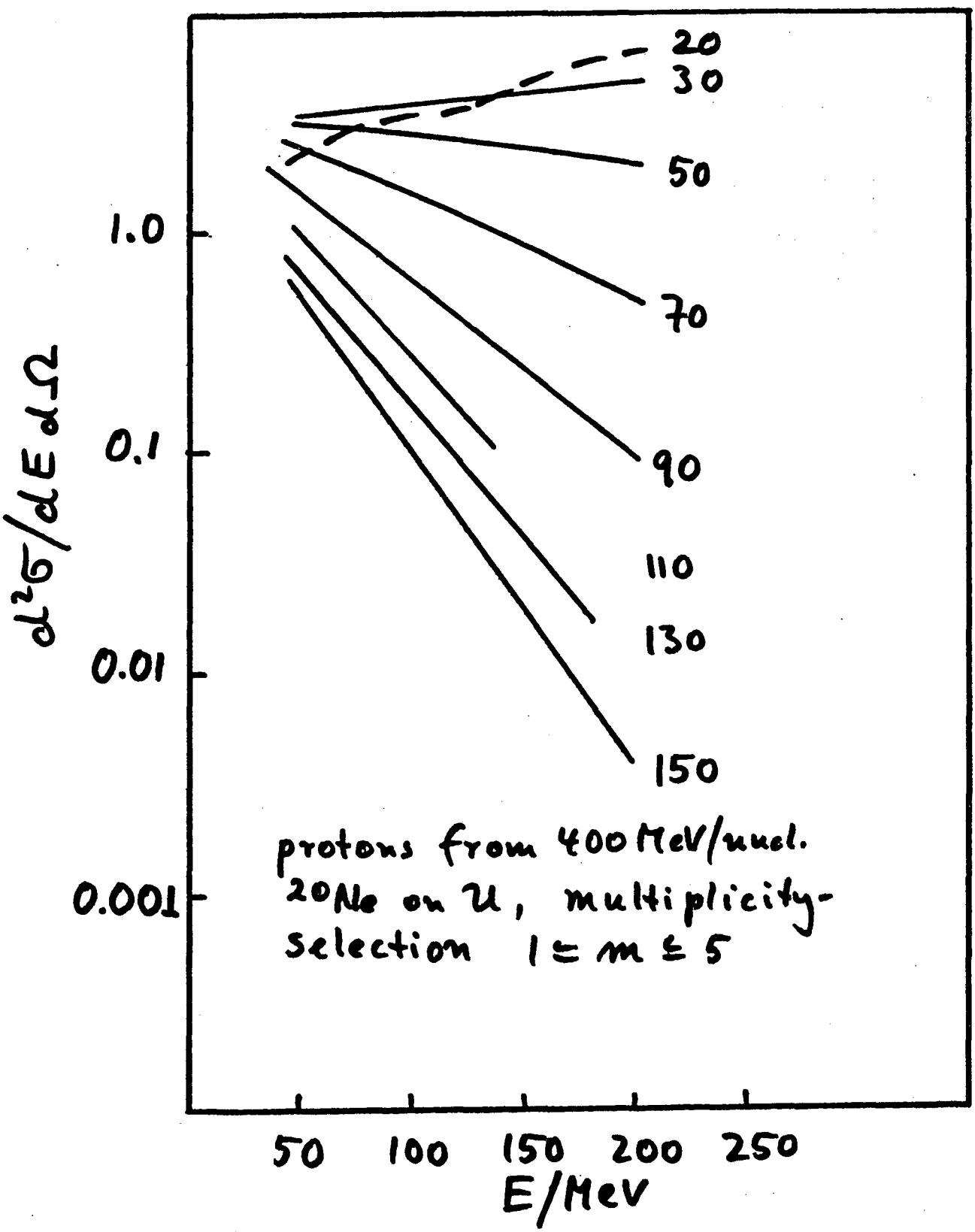
20
30
50
70
90
110
130
150
1.0
0.1
0.01
0.001
$d^2\sigma/dE\,d\Omega$
protons from 400 MeV/nucl.
^{20}Ne on U, multiplicity-
selection $1 \leq m \leq 5$
50
100
150
200
250
E/MeV

Fig 25 b

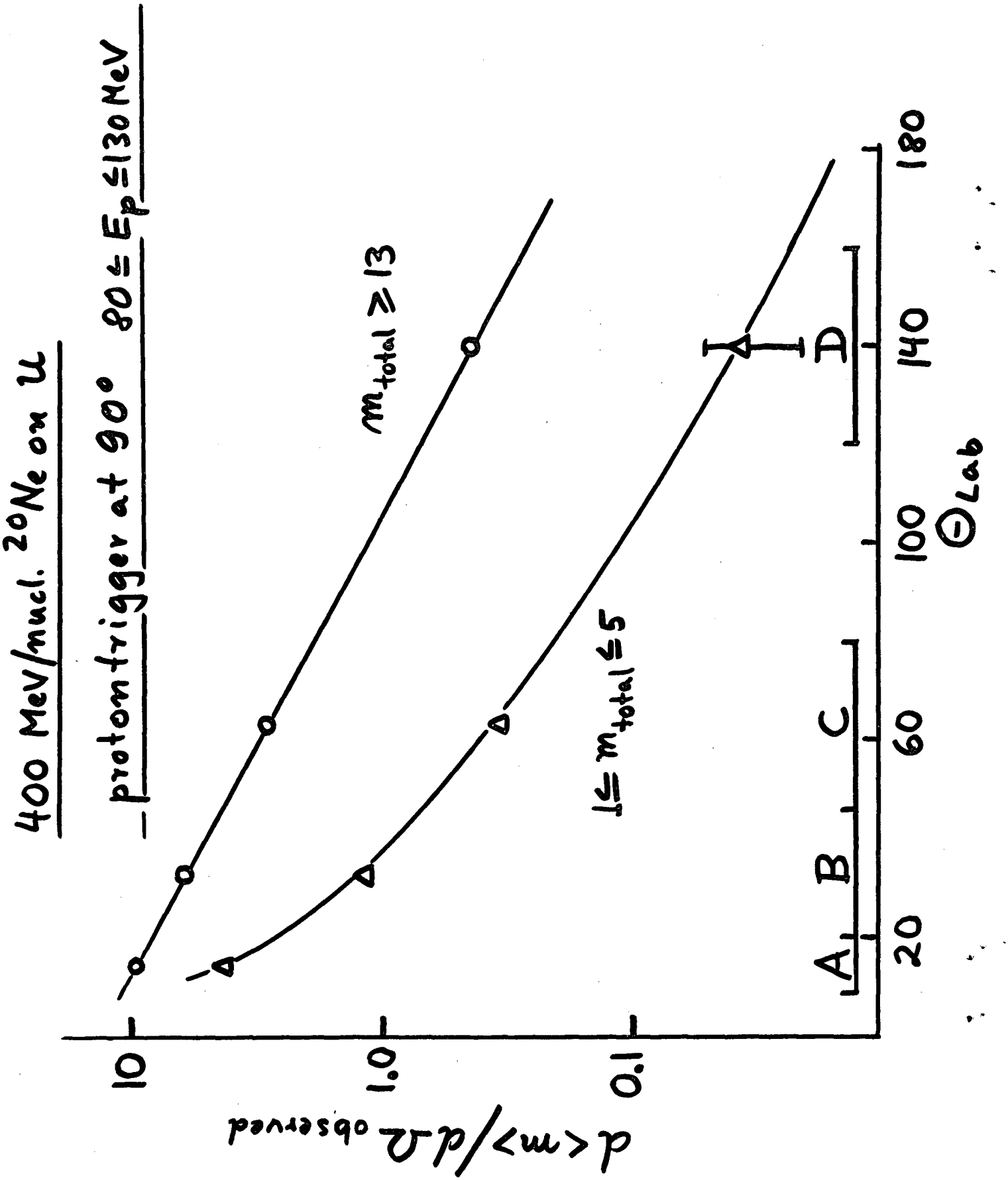
400 MeV/nucl. ^{20}Ne on U
protontrigger at 90° 80 ≤ E_p ≤ 130 MeV
$m_{total} \geq 13$
$1 \leq m_{total} \leq 5$
$d\langle m\rangle/d\Omega$ observed
10
1.0
0.1
20
60
100
140
180
Θ_{Lab}
A
B
C
D

Fig 26

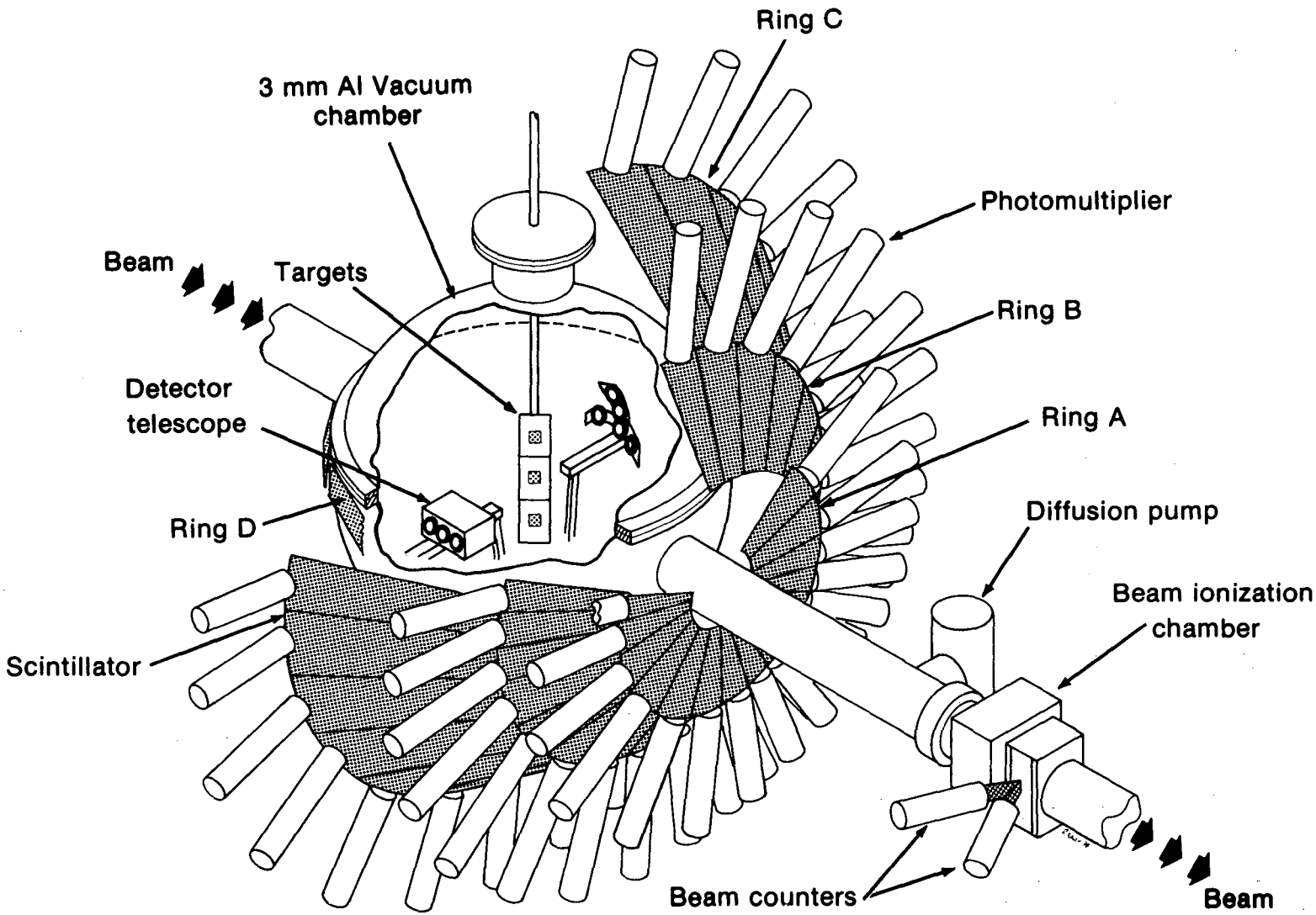
Ring C
3 mm Al Vacuum chamber
Photomultiplier
Beam
Targets
Ring B
Detector telescope
Ring A
Ring D
Diffusion pump
Beam ionization chamber
Scintillator
Beam counters
Beam
XBL 782-7229 D

Fig. 27

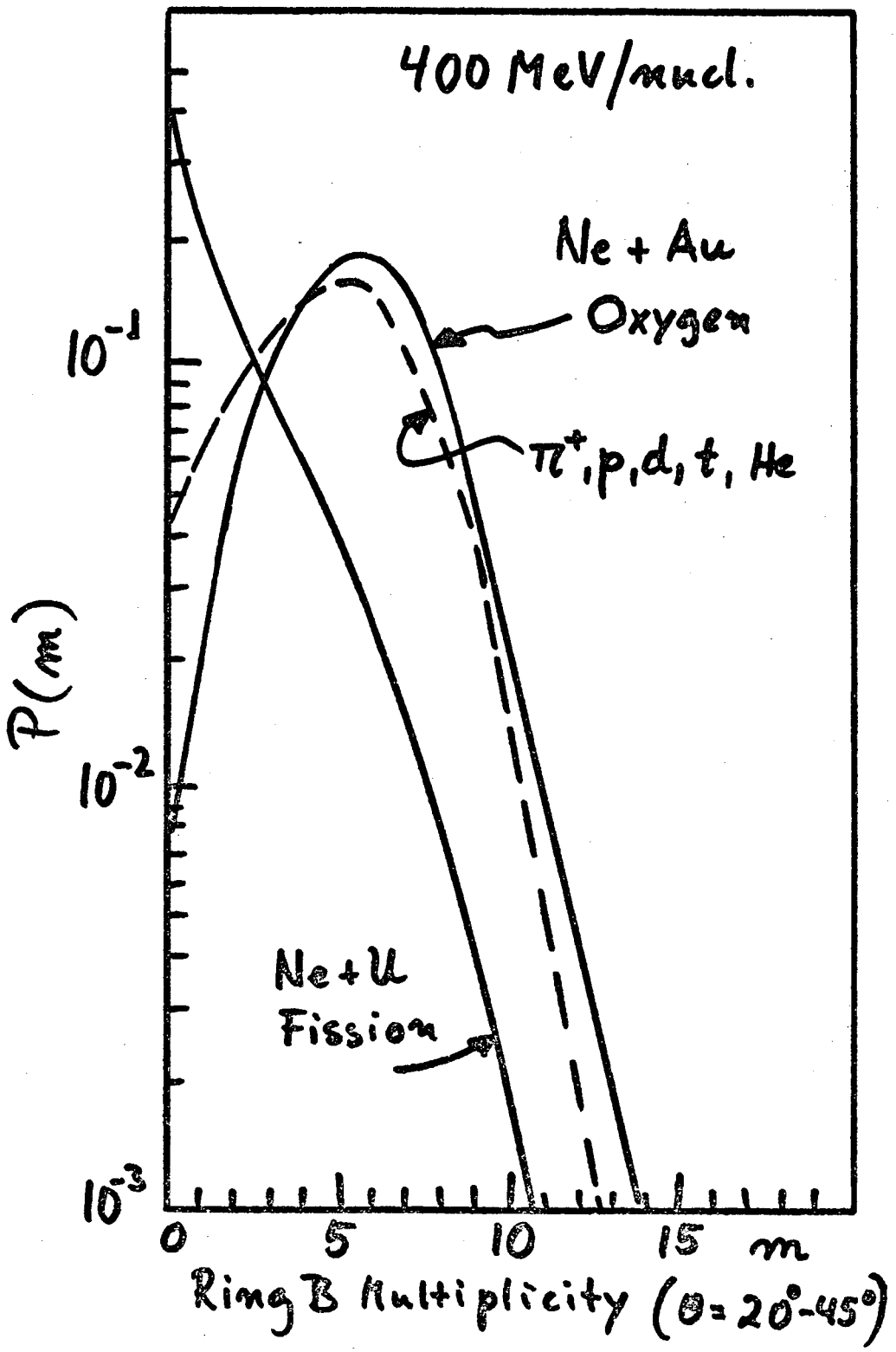
400 MeV/nucl.
Ne + Au
Oxygen
π+, p, d, t, He
Ne + U
Fission
P(m)
10-1
10-2
10-3
0
5
10
15
m
Ring B Multiplicity (θ = 20°-45°)

Fig 28

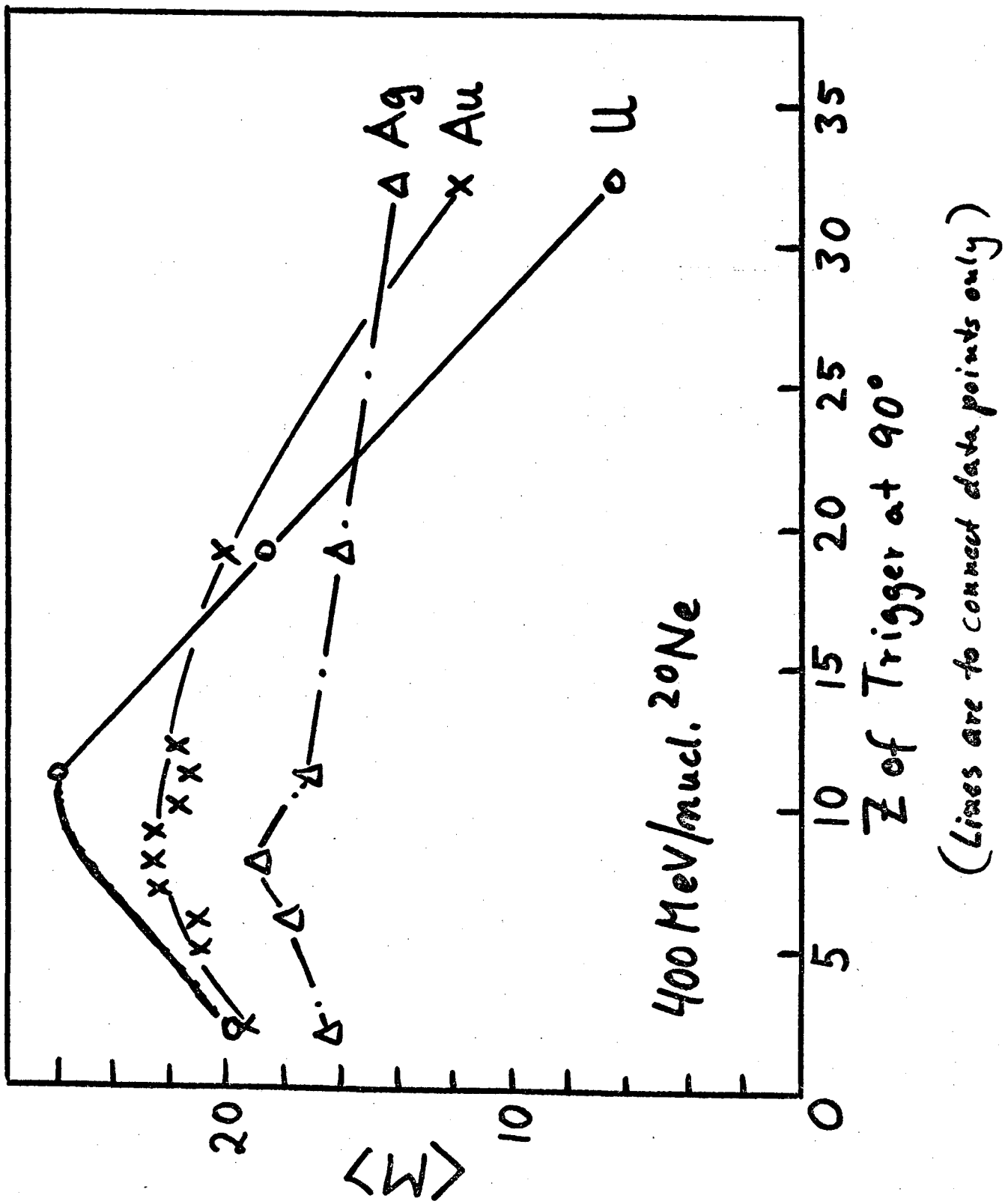
Δ Ag
x Au
o U
400 MeV/nucl. ^{20}Ne
Z of Trigger at 90°
(Lines are to connect data points only)
⟨M⟩
0
5
10
15
20
25
30
35
10
20

Fig. 29

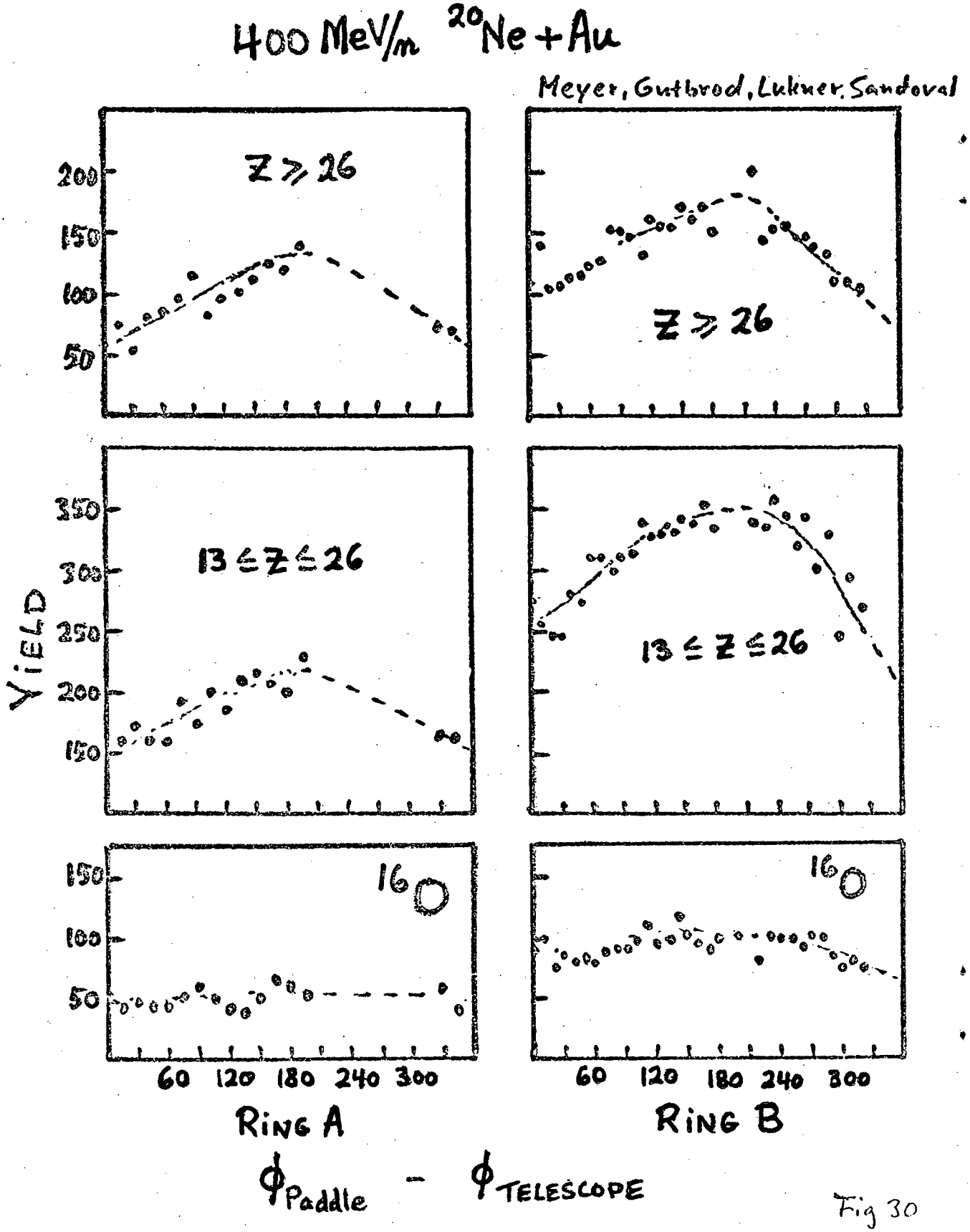
400 MeV/n 20Ne + Au
Meyer, Gutbrod, Lukner, Sandoval
Z ≥ 26
Z ≥ 26
13 ≤ Z ≤ 26
13 ≤ Z ≤ 26
16O
16O
YIELD
200
150
100
50
350
300
250
200
150
150
100
50
60 120 180 240 300
60 120 180 240 300
RING A
RING B
φPaddle - φTELESCOPE

Fig 30

TECHNICAL INFORMATION DEPARTMENT
LAWRENCE BERKELEY LABORATORY
UNIVERSITY OF CALIFORNIA
BERKELEY, CALIFORNIA 94720